Bull. Disas. Prev. Res. Inst., Kyoto Univ., Vol. 29, Part 4, No. 267, March, 1980

Studies on the Structures of Density Stratified Flows

By Shinji EGASHIRA and Kazuo ASHIDA

(Manuscript received December 27, 1979)

Abstract

Density stratified flows are classified into three classes such as upper, middle and under layer flows. In this study, the time averaged mean profiles of velocity, density and temperature are discussed in stably stratified media, and also the theories of turbulent diffusion coefficients for momentum, mass and heat are developed.

We consider the mixing length l_0 at a density interface and assume a linear distribution of the mixing length in main flow region, and then theories of velocity profiles are established. Those of density and temperature profiles are also developed, assuming the distributions of mixing lengths for mass and heat respectively. The effects of density stratification in these profiles are evaluated by the changes of the distributions of the mixing lengths for momentum, mass and heat from the distributions in neutral stability.

Turbulent diffusion coefficients for mass and heat are discussed directly on the basis of mixing length theory and predictive methods on them are presented.

The theories developed in this paper show good agreement with the experiments.

1. Introduction

In analysis of transport phenomena, there are two requests as follows. One is the case that it is enough for us to know the cross-sectional mean of a given hydraulic quantity. The other is that we must analyze the distributions of velocity, density, temperature, turbidity and so on in the whole flow region.

Fig. 1 shows two methods to treat the transport phenomena relating to density

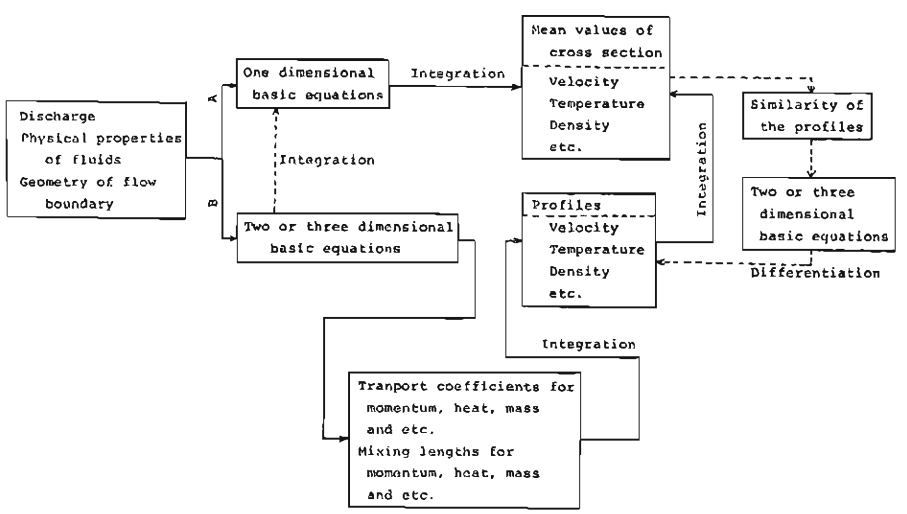

Fig. 1. A flow chart to solve the transport phenomena of density stratified flows.

stratified flows. Along A in the figure, one dimensional governing equations are applied to solve the phenomena, and it is important how to formulate the mass and momentum transports around a flow boundary such as a density interface. The method of direction B is the one in which the profiles of hydraulic quantities are discussed with two or three dimensional basic equations. We usually get the solution under some approximations like boundary layer assumption because the governing equations are very rarely directly integrated.

Lets introduce parts of the investigations concerning the later case except numeric methods. On turbulent shear flow and the relating phenomena very near the atmospheric surface, many field experiments have been carried since Monin·Obukhov similarity theory[1] (1954) was presented, and log-linear law has been applicable to wind velocity, air temperature and moisture in the region except strong stability range (McVehill[2], 1964; Webb[3], 1970). On the other hand, few analytical procedures have been carried concerning the phenomena inner and over the miscible density interface formed by the abrupt changes of temperature and solute concentration because it is very difficult to decide the transfer condition at an interface and the distribution of transport coefficients in a flow region. Recently, theories of the profiles of velocity and water density distributions in a two dimensional definite region were presented by the authors[4)~6)] (1977–1979) and Hino[7] (1979). The difference between these theories is in the assumptions which are introduced to analyze the flow near an interface.

Transport coefficients for momentum, heat and some solutions for stratified shear flows had been studied for a long time, and many empirical and theoretical relations had been presented. The formula presented by Munk·Anderson[8] (1948) is very well known and applied to analyze the phenomena nowadays. Ellison[9] (1957) and Ellision·Turner[10] (1960) obtained the formula using the governing equations of turbulence. But the diffusion term for pressure fluctuation was omitted in the theoretical procedure. On the other hand, Launder[11] (1975) presented a theory for transport coefficient, considering the pressure term. When one compares the transport coefficients calculated by these formulae including the preceding similarity theory, it will be found that the characteristic of each formula is different from each other. The differences will become remarkable if one investigates how to change the ratio of transport coefficients with the stability parameter such as gradient Richardson number. One of the reasons of this discrepancy between these formulae will be because of each formula developed different stratified systems.

As mentioned above, there are a number of unsolved problems regarding the velocity profile and other quantities in stably stratified shear flows. The purpose of the present study is to reveal the velocity, density and temperature profiles and the transport coefficients in density stratified shearing flows which will be formed in man-made reservoirs and estuaries. At first, the relation between turbulent entrainment coefficient and eddy diffusivity for mass and heat is described by use of the mass conservation equations in discrete and continuous stratified systesms Laws of profiles of time-averaged mean quantities are derived from the mixing length theory under the assumption of constant flux layer. Transport coefficients are discussed by the distributions of mixing lengths obtained here. Lastly, the theories presented will be compared with experiments of upper and middle layer flows.

2. Relation between Turbulent Entrainment Coefficient and Eddy Diffusion Coefficient for Mass and Heat

An upper layer flow is shown schematically, and profiles of velocity and water density in two layer and continuous stratified systems are described respectively in **Fig. 2**. For a two layer model, a mass conservation equation can be written as follows.

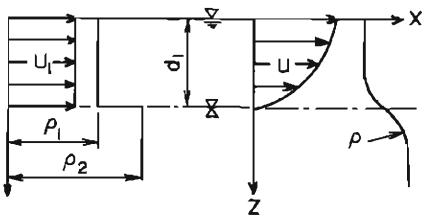

Fig. 2. Two layered and continuous density stratified systems.

$$\frac{\partial \rho_1}{\partial t}+U_1\frac{\partial \rho_1}{\partial x}=\frac{\Delta\rho}{d_1}W_e \tag{1}$$

where ρ_1 is water density in the upper layer, $\Delta\rho$: $\rho_2-\rho_1$ (ρ_2: water density in the under layer), U_1: mean velocity in cross section, d_1: water depth in the upper layer and W_e: entrainment velocity.

Mass conservation for a continuous system of two dimensions is written by a convected diffusion equation as

$$\frac{\partial \rho}{\partial t}+\frac{\partial}{\partial x}(\rho u)+\frac{\partial}{\partial z}(\rho w)=\frac{\partial}{\partial x}\left(\varepsilon_{\rho x}\frac{\partial \rho}{\partial x}\right)+\frac{\partial}{\partial z}\left(\varepsilon_{\rho z}\frac{\partial \rho}{\partial z}\right). \tag{2}$$

Where t is time, x and z: coordinate system as shown in Fig. 2, ρ: time mean water density, u and w: time mean velocity in x and z components respectively, $\varepsilon_{\rho x}$ and $\epsilon_{\rho z}$: x and z components of eddy diffusion coefficient for mass respectively. The first term of the right hand side of equation (2) is usually negligibly small, and can be cancelled. As to ρ and u in the first and the second terms of the left, the following procedure is taken up. These quantities can be written in terms of the cross sectional mean and the variation from them.

$$\left.\begin{aligned}\rho&=\rho_1+\rho''\\ u&=U_1+u''\end{aligned}\right\} \tag{3}$$

Integrating equation (2) from surface ($z=0$) to interface ($z=d_1$) using equation (3), one can obtained the following relation.

$$\begin{aligned}&\rho_1\left\{\frac{\partial d_1}{\partial t}+\frac{\partial}{\partial x}(U_1 d_1)\right\}+d_1\left(\frac{\partial \rho_1}{\partial t}+U_1\frac{\partial \rho_1}{\partial x}\right)+\rho_1(d_1,t)\left\{\frac{\partial d_1}{\partial t}\right.\\&\left.+u(d_1,t)\frac{\partial d_1}{\partial x}-w(d_1,t)\right\}=\varepsilon_{\rho z}(d_1,t)\frac{\partial \rho}{\partial z}\Big|_{z=d_1}-\varepsilon_{\rho z}(0,t)\frac{\partial \rho}{\partial z}\Big|_{z=0}\end{aligned} \tag{4}$$

Where $\rho(d_1, t)$, $u(d_1, t)$ and $w(d_1, t)$ are time averaged quantities at the interface, respectively. $w(d_1, t)$ and the first term of equation (4) can be described in terms of entrainment velocity as follows.

$$w(d_1, t)=\frac{\partial d_1}{\partial t}+u(d_1, t)\frac{\partial d_1}{\partial x}-W_e \tag{5}$$

$$W_e=\frac{\partial d_1}{\partial t}+\frac{\partial}{\partial x}(U_1 d_1) \tag{6}$$

Water density $\rho(d_1, t)$ at the interface will be well approximated by

$$\rho(d_1, t)=(\rho_1+\rho_2)/2\,. \tag{7}$$

Assuming mass or heat transfer is negligible at the free surface, which can be written as $\varepsilon_{\rho z}\partial\rho/\partial z|_{z=0}=0$, and rearranging equation (4) by use of equations (5), (6) and (7), the new expression for eddy diffusion coefficient at an interface is derived as follows.

$$\varepsilon_{\rho z}(d_1, t)=\frac{\Delta\rho}{2(\partial\rho/\partial z)_i}W_e \quad (=\varepsilon_{\rho i}) \tag{8a}$$

where $(\partial\rho/\partial z)_i$ and $\varepsilon_{\rho i}$ are density gradient and eddy diffusion coefficient at an interface, respectively. In case that z-axis is selected upward from the interface,

$$\varepsilon_{\rho i}=-\frac{\Delta\rho}{2(\partial\rho/\partial z)_i}W_e\,. \tag{8b}$$

Thus the relation between eddy diffusion coefficient for mass and entrainment velocity has been obtained. Concerning the relation between eddy diffusion coefficient for heat and entrainment velocity, an equation as well as (8a) or (8b) could be led through the same procedure as mentioned above. Here we would like to show the results only:

$$\varepsilon_{Hi}=-\frac{T_1-T_2}{(\partial T/\partial z)_i}W_e \tag{9}$$

where ε_{Hi} is eddy diffusion coefficient for heat at the interface, $(\partial T/\partial z)_i$: temperature gradient at the interface, T_1 and T_2: cross sectional means of temperature in upper and under layers respectively. Comparing equations (8a) with (9), it could be found that eddy diffusion coefficients are the same as in the linear range of heat expansion coefficient of water.

The hydraulic characteristic of equation (8a) will become clear if we consider the hydraulic variables of the entrainment velocity and the density gradient at an interface. The discussion as to density gradient will be taken up in the next chapter. Let us relate the entrainment velocity briefly. The term is usually written by use of the entrainment coefficient E as follows.

$$W_e=EU_1 \tag{10}$$

Many experimental investigations have been done as to entrainment coefficients. According to these studies (Kato·Phillips[12], 1967; Moore·Long[13], 1971; Ashida·Egashira[14], 1977) and to much data of other experiments (Lofquist[15], 1960), it was

found that the coefficient was proportional to the inverse of the overall Richardson number.

$$E=K/R_{i*} \tag{11}$$

where K is the coefficient to be decided by experiment and R_{i*}: overall Richardson number defined by

$$R_{i*}=F_i^{-2}=\frac{\Delta\rho}{\rho}gd_1/U_1^2\,. \tag{12}$$

In **Fig. 3**, data obtained by Ellison·Terner[16] (1959), Lofquist, Kato·Phillips and

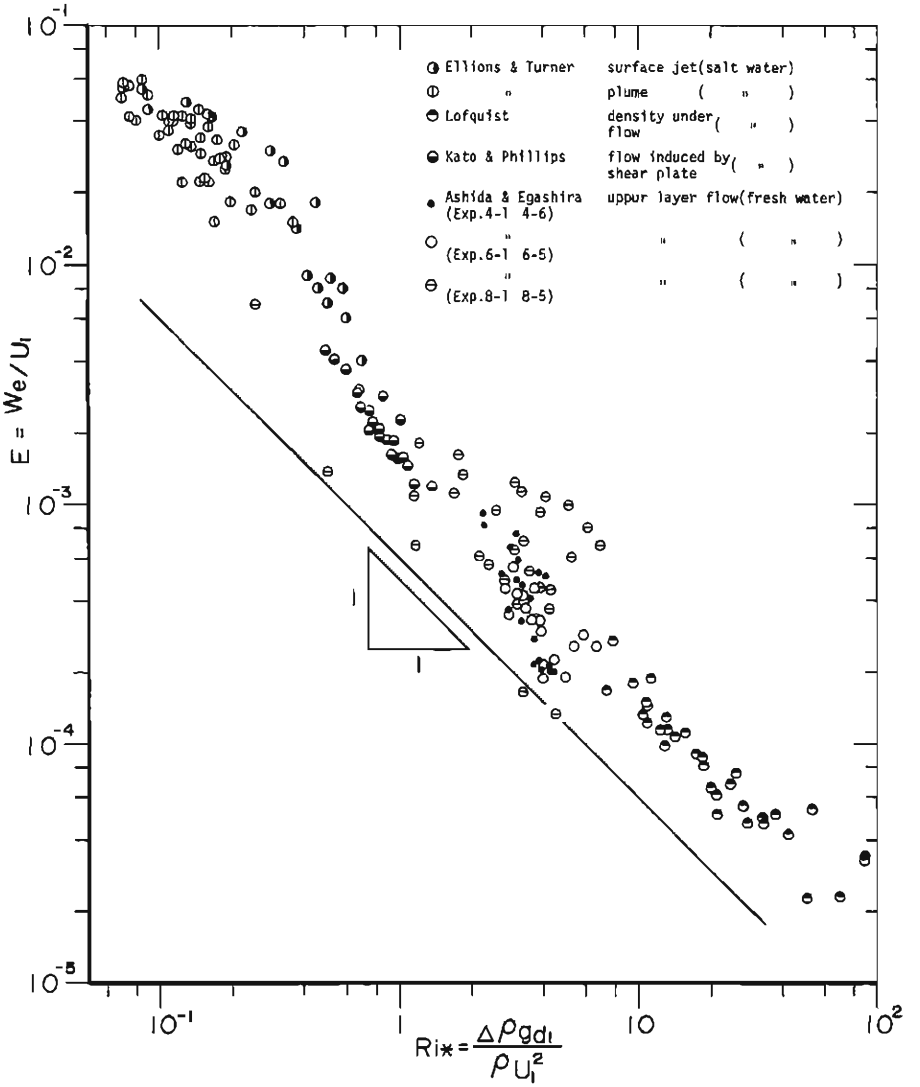

Fig. 3. Turbulent entrainment coefficient and overall Richardson number.

Ashida·Egashira are shown. The entrainment coefficient would be considered to be well defined by equation (11), and most data could be represented by the factor of

$$K=0.0015. \tag{13}$$

Rearranging equation (8a) by use of equation (11), eddy diffusion coefficient at the density interface is written as below.

$$\varepsilon_{\rho i}=\frac{\Delta\rho}{2(\partial\rho/\partial z)_i}\frac{KU_1}{R_{i*}} \tag{14}$$

This equation shows that the eddy diffusion coefficient becomes large with the increase of turbulent entrainment.

3. Velocity Profiles of Density Stratified Flows

3.1 Velocity Profiles

(1) Upper Layer Flow

Filling water with homogeneous density into a prismatic channel to the level of a weir top, an upper layer flow can be formed easily if one constantly supplies the water of lower density at the upstream end and has the water overflow the weir. Using two fluids of which temperature only is different, the upper layer flow formed by the method mentioned above is shown, and its velocity and temperature profiles are also shown schematically in **Fig. 4**. Although the density interface lowers with time, the profiles remain unchanged.

Concerning the upper layer flow as shown in Fig. 4, we would like to discuss

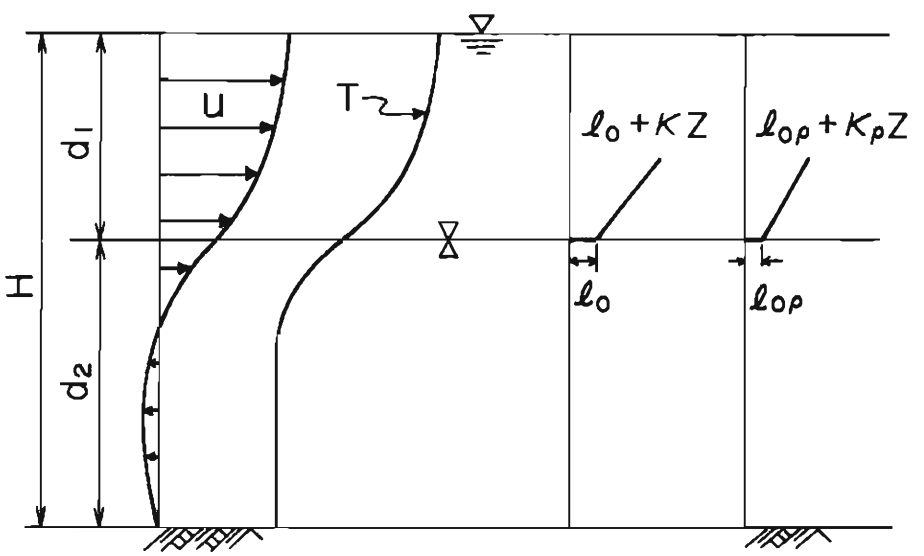

Fig. 4. The schematic diagram for an upper layer flow and the distributions of mixing lengths for momentum and mass density.

its velocity profile on the basis of Prandtl mixing length theory for momentum. We suppose the mixing length in main flow region as below (Ashida·Egashira[17], 1975).

$$l = l_0 + \kappa z \tag{15}$$

where l_0 is the mixing length at the interface ($z=0$) and κ: Kármán constant. The velocity gradient can be described as

$$\frac{du}{dz} = \frac{u_*}{l_0 + \kappa z} = \frac{u_*}{d_1(\beta + z/d_1)} \tag{16}$$

, where u_* is the shear velocity and β: nondimensional mixing length at the interface.

$$\beta = l_0/d_1 \tag{17}$$

Integrating equation (16) under constant flux layer leads to

$$u(\zeta) = u_i + \frac{u_*}{\kappa} \ln \frac{\beta + \kappa\zeta}{\beta}, \quad (0 \leq z \leq d_1 \text{ or } 0 \leq \zeta \leq 1) \tag{18}$$

, where ζ is defined by z/d_1. The velocity u_i at the interface can be obtained from the condition of continuity as below.

$$u_i = \frac{q}{d_1} - u_* \left(\frac{\beta + \kappa}{\kappa^2} \ln \frac{\beta + \kappa}{\beta} - \frac{1}{\kappa} \right) \tag{19}$$

where q: discharge in unit width. The velocity profile of the main flow region having been described, we would like to discuss the velocity in the lower region between interface and channel bed. A kind of circulating flow will be formed due to the definite flow field, which currents in the same direction of the main flow near the interface and in the opposite near the bed. Although it is very difficult for us to discuss the velocity distribution in such a circulating flow, but the curve of a quadratic equation as shown below will give a good approximation to it except near the upstream and downstream regions.

$$u = a_1 \zeta'^2 + a_2 \zeta' + a_3, \quad (\zeta' = -z/d_2) \tag{20}$$

where d_2 is the lower layer depth. a_1, a_2 and a_3 in equation (20) will be decided by the following conditions.

$$\zeta' = 0, \; u = u_i \tag{21}$$

$$\zeta' = 1, \; u = 0 \tag{22}$$

$$\int_0^1 u \, d\zeta' = 0 \tag{23}$$

Using the factors decided by equation (21) to (23), one can get the velocity profile in the under layer:

$$u(\zeta') = (3\zeta'^2 - 4\zeta' + 1)u_i, \; (-d_2 \leq z \leq 0 \text{ or } 0 \leq \zeta' \leq 1). \tag{24}$$

This equation indicates that $u=0$ at $\zeta' = 1/3$, and the maximum inverse flow occurs at $\zeta' = 2/3$ as $u = -u_i/3$.

(2) Middle Layer Flow

Here we will define a middle layer flow in a two dimensional definite region as follows. The main flow region is formed between two density interfaces, and weak circulating currents are formed in the upper layer over the first interface and in the lower layer between the second interface and the channel bed. Such kind of density stratified flow is schematically shown in **Fig. 5**. In the case of middle layer flow, we will be able to discuss its velocity distribution by the foregoing method.

As shown in **Fig. 5**, we select y-axis downwards from the first interface and z-axis upwards from the second interfaces, and suppose that the distributions of mixing length for momentum are put as follows.

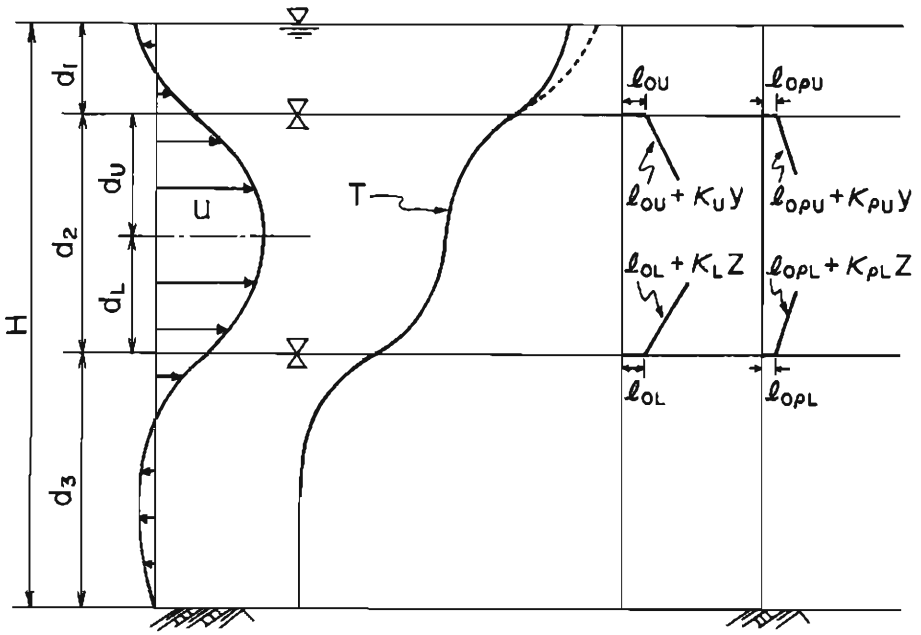

Fig. 5. The schematic diagram for a middle layer flow and the distributions of mixing lengths for momentum and mass density.

$$l(y)=l_{0U}+\kappa_U y \tag{24}$$

$$l(z)=l_{0L}+\kappa_L z \tag{25}$$

Where l_{0U} and l_{0L} are the mixing lengths at the first and the second interfaces respectively, κ_U and κ_L: Kármán constants. Using equations (24) and (25), the velocity gradients can be described below, respectively.

$$\frac{du}{dy}=\frac{u_{*U}}{l_{0U}+\kappa_U y}=\frac{u_{*U}}{d_U(\beta_U+\kappa_U y/d_U)} \tag{26}$$

$$\frac{du}{dz}=\frac{u_{*L}}{l_{0L}+\kappa_L z}=\frac{u_{*L}}{d_L(\beta_L+\kappa_L z/d_L)} \tag{27}$$

Where u_{*U} and u_{*L} are shear velocities, d_U and d_L: the depths from each interface

to the point of maximum velocity, β_U and β_L: the dimensionless mixing lengths at two interfaces defined below.

$$\beta_U = l_{0U}/d_U \tag{28}$$

$$\beta_L = l_{0L}/d_L \tag{29}$$

By integrating equations (26) and (27) under the condition of constant flux layer, the velocity profiles of main flow region are obtained respectively as follows.

$$u(\eta) = u_{max} - \frac{u_{*U}}{\kappa_U} \ln \frac{\beta_U + \kappa_U}{\beta_U + \kappa_U \eta} \tag{30}$$

$$u(\zeta) = u_{max} - \frac{u_{*L}}{\kappa_L} \ln \frac{\beta_L + \kappa_L}{\beta_L + \kappa_L \zeta} \tag{31}$$

Where $\eta = y/d_U$, $\zeta = z/d_L$, and u_{max}: the maximum velocity. From the condition of continuity,

$$d_U \int_0^1 u(\eta)\, d\eta + d_L \int_0^1 u(\zeta)\, d\zeta = q \tag{32}$$

, the maximum velocity can be obtained:

$$u_{max} = \frac{q}{d_2} + \frac{u_{*U}}{\kappa_U^2}\left(\kappa_U - \beta_U \ln \frac{\beta_U + \kappa_U}{\beta_U}\right)\frac{d_U}{d_2} + \frac{u_{*L}}{\kappa_L^2}\left(\kappa_L - \beta_L \ln \frac{\beta_L + \kappa_L}{\beta_L}\right)\frac{d_L}{d_2}. \tag{33}$$

Where q is discharge in unit width, and d_2 $(= d_U + d_L)$: the depth of main flow region. Using friction coefficients defined by $f_{iU} = 2(u_{*U}/U_2)^2$ and $f_{iL} = 2(u_{*L}/U_2)^2$ where U_2 is the mean velocity of main flow, and supposing the linearity of shear stress, the depth ratios in equation (33) become the following.

$$d_U/d_2 = f_{iU}/(f_{iU} + f_{iL}) \tag{34}$$

$$d_L/d_2 = f_{iL}(f_{iU} + f_{iL}) \tag{35}$$

Concerning the velocity profiles in both sides of a main flow region, those will be discussed in the same manner as in the upper layer flow. In the layer ranging from $y = -d_1$ to $y = 0$, the coefficients of a quadratic equation can be decided by the next three conditions.

$$y = -d_1 \text{ (free surface)}, \quad du/dy = 0 \tag{36}$$

$$y = 0 \text{ (the first interface)}, \quad u = u_{iU} \tag{37}$$

$$\int_{-d_1}^{0} u\, dy = 0 \tag{38}$$

In the layer ranging from $z = -d_3$ to $z = 0$, those conditions are as follows.

$$z = -d_3 \text{ (channel bed)}, \quad u = 0 \tag{39}$$

$$z = 0 \text{ (the second interface)}, \quad u = u_{iL} \tag{40}$$

$$\int_{-d_3}^{0} u\, dz = 0 \tag{41}$$

By using equations from (36) to (41), the velocity profiles in each layer can be obtained as follows.

$$u(\eta')=(3/2\eta'^2-3\eta'+1)u_{iU}, \quad (-d_1\leq y\leq 0 \text{ or } 0\leq\eta'\leq 1) \tag{42}$$

$$u(\zeta')=(3\zeta'^2-4\zeta'+1)u_{iL}, \quad (-d_3\leq z\leq 0 \text{ or } 0\leq\zeta'\leq 1) \tag{43}$$

Where η' and ζ' are defined as $\eta'=-y/d_1$ and $\zeta'=-z/d_3$ respectively. Velocities at the two interfaces are obtained from equations (30) and (31) as below.

$$u_{iU}=u_{max}-\frac{u_{*U}}{\kappa_U}\ln\frac{\beta_U+\kappa_U}{\beta_U} \tag{44}$$

$$u_{iL}=u_{max}-\frac{u_{*L}}{\kappa_L}\ln\frac{\beta_L+\kappa_L}{\beta_L} \tag{45}$$

Concerning density stratified flows in stable stratification, the velocity profiles in upper and middle layer types have been discussed. Shear velocities, nondimensional mixing lengths at interfaces and Kármán constants play an important role in these theories. We would like to take up the latter two in other sections. In order to predict the shear velocity at an interface, one usually employs the equation of shear stress coefficient. Although many relations on it have been presented, there are too few to be able to use universally. Here we would like to introduce the only result developed theoretically by Egashira·Ashida[6] (1979). In the upper layer flow,

$$f_i=\frac{A}{R_e}+0.00207F_i^2+0.0015\frac{H-d_1}{H} \tag{46}$$

, where f_i is the shear stress coefficient defined by $f_i=2(u_*/U_1)^2$, R_e: Reynolds number, F_i: internal Froude number shown in equation (12), H and d_1: shown in **Fig. 4**. Although A in equation (46) can be led to the factor of 1.86 theoretically in two dimensional flow, $A\fallingdotseq 15$ is obtained from data fitting. The discrepancy between these factors is considered due to the side effects of channels.

Equation (46) will be able to extend easily to the case of middle layer flow as follows.

$$f_{iU}=A/R_e+0.00207F_{iU}^2+0.0015\,d_1/(d_1+d_2) \tag{47}$$

$$f_{iL}=A/R_e+0.00207F_{iL}^2+0.0015\,d_3/(d_2+d_3) \tag{48}$$

Where F_{iU} and F_{iL} are the internal Froude number defined by the quantities between the main flow region and the other ones, d_1, d_2 and d_3: shown in **Fig. 5**.

3.2 Nondimensional Mixing Length at Interface

The interface will exhibit a strong stability due to the density gradient. Webb[3] (1970) indicated that the velocity gradient was evaluated by the following equation as the limit of the log-linear law.

$$\frac{du}{dz}=\frac{\alpha u_*}{\kappa_N L} \tag{49}$$

where κ_N is Karman's universal constant (0.4), α: an empirical constant to be decided,

and L: Monin·Obukhov length. Equation (49) means the velocity field is controlled only by momentum and heat or mass flux. In this condition, which is called self-regulated state (Turner[18], 1973), the velocity changes linearly. The linearity of a velocity profile could be found in the interface regions of inclined plume carried out by Ellison·Turner[16] (1959), turbidity current by Ashida·Egashira[17] (1975) and surface jet by Komatsu[19] (1978). These experimental facts say that the flows near a density interface are in the condition of a self-regulated state. Rewriting the above expression according to Turner[18] (1973), equation (49) becomes

$$\partial u/\partial z = k_1 g\overline{\rho' w'}/\rho u_*^2 . \tag{50}$$

Where k_1 is the empirical constant to be decided. $\overline{\rho' w'}$, which is turbulent mass flux in vertical direction, can be written as

$$\overline{\rho' w'} = -\varepsilon_{\rho i}(\partial\rho/\partial z)_i . \tag{51}$$

By substituting $\varepsilon_{\rho i}$ for equation (14), the above relation is transformed into

$$\overline{\rho' w'} = 1/2 \cdot K \Delta\rho U_1/R_{i*} . \tag{52}$$

From equation (16), the velocity gradient at an interface can be described as follows.

$$\partial u/\partial z = u_*/l_0 \tag{53}$$

From equations (50), (52) and (53), nondimensional mixing length at interface is obtained:

$$\beta = l_0/d_1 = \gamma_1 (U_1/u_*)^{-3} \tag{54}$$

, where γ_1 is the constant to be decided experimentally and can be written by K and k_1 as follows.

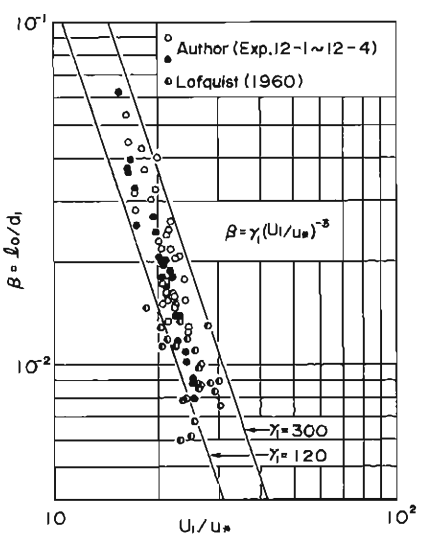

Fig. 6. The relation between velocity coefficient and nondimensional mixing length at a density interface for momentum.

$$\gamma_1 = 2(k_1 K)^{-1} \tag{55}$$

In Fig. 6, the relation is shown between equation (54) and much data obtained from channel experiments (Lofquist[15], 1960; Egashira·Ashida[6], 1979). It will be found that the trend of these data is represented well by equation (54), and most data lies in the range of

$$120 \leq \gamma_1 \leq 300 . \tag{56}$$

Concerning an upper layer flow, the nondimensional mixing length for momentum has been discussed. We can easily extend equation (54) or the relation shown in Fig. 6 to the case of middle layer flow. That is, by using U_2, u_{*U} and u_{*L} instead of U_1 and u_*, the nondimensional mixing lengths defined by β_U and β_L at the first and the second interfaces are shown below.

$$\beta_U = \gamma_1 (U_2/u_{*U})^{-3} \tag{57}$$

$$\beta_L = \gamma_1 (U_2/u_{*L})^{-3} \tag{58}$$

3.3 Kármán Constant in Stably Stratified Flows

The influence of density stratification on the log-linear law for the wind velocity is evaluated by the Monin·Obukhov function. For the density stratified flows taken up here, we would like to discuss the change of Kármán constant, that is, the change of the mixing length in the main flow region by use of the acceleration balance equation proposed by Kao[20] (1959). Kao's equation for the case of the upper layer flow shown in Fig. 4, can be transformed into

$$l\left(\frac{du}{dz}\right)^2 = l_N\left(\frac{du}{dz}\right)^2 + B\frac{g}{\rho} l_\rho \frac{d\rho}{dz} \tag{59}$$

, where l_N is the mixing length for mass and B: a proportional constant. By using equations (52) and (68) which express the mass flux and the density gradient respectively, equation (59) can be written as

$$l\left(\frac{du}{dz}\right)^2 = l_N\left(\frac{du}{dz}\right)^2 - \frac{1}{2} BKg' \frac{1}{R_{i*}} \frac{U_1}{u_*} \tag{60}$$

, where $g' = \Delta\rho/\rho \cdot g$. The acceleration balance equation having been obtained, we will investigate the change of Kármán constant in accordance with Hino's method[21] (1963) concerning the two phase flow.

Putting the velocity gradient as

$$du/dz = u_*/l = u_*/l_N \cdot \psi, \ (\psi = l_N/l) \tag{61}$$

, and substituting equation (61) for du/dz in equation (60), the acceleration balance equation becomes

$$\frac{u_*^2}{l_N}\psi = \frac{u_*^2}{l_N}\psi^2 - \frac{1}{2} BKg' \frac{1}{R_{i*}} \frac{U_1}{u_*} . \tag{62}$$

If we fix our object in the region where $l_0 + \kappa z$ is nearly equal to κz, the mixing length ratio will be

$$\psi = \frac{l_{0N} + \kappa_N z}{l_0 + \kappa z} = \frac{\kappa_N}{\kappa} \tag{63}$$

, where suffix-N means neutral stability. The above relation indicates that ψ is independent of z. By integrating equation (62) from the interface ($z=0$) to the surface ($z=d_1$), the quadratic equation with respect to ψ is obtained as follows.

$$\psi^2 - \psi - \frac{1}{2}\frac{B}{B'}\frac{K}{R_{i*}}\frac{U_1}{u_*}\frac{g'd_1}{u_*^2} = 0 \tag{64}$$

, where

$$B' = \frac{1}{\kappa_N}\ln\frac{\beta_N + \kappa_N}{\beta_N} = \text{const.}$$

Putting $\kappa_N = 0.4$ and supposing that β_N is the same order as β, B' becomes about one. Rewriting B/B' as B including B' consequently, one can get the solution of equation (64):

$$\frac{\kappa}{\kappa_N} = \frac{2}{1+\sqrt{1+2BK(U_1/u_*)^3}}\,. \tag{65}$$

Applying equation (46) to U_1/u_*, we can find an interesting feature. With a large Reynolds Number, the Kármán constant will be regulated by an internal Froude number only. It will approach its neutral condition as the mixing action gets large with increase of Froude number.

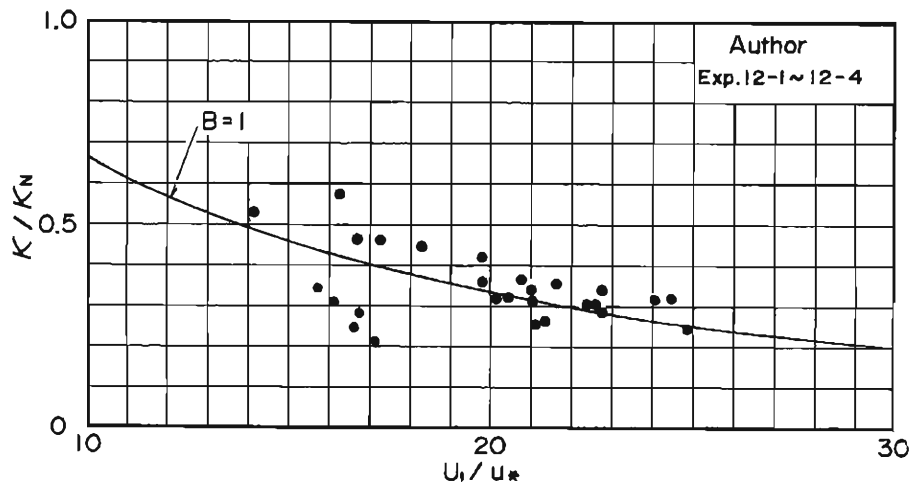

Fig. 7. The relation between the velocity coefficient and the ratio of Kármán constants. Where κ is Kármán constant in stably stratified media and $\kappa_N(=0.4)$ is the one in neutral stability concerning the mixing length for momentum.

Fig. 7 shows the relation between the curve calculated by equation (65) with $B=1$ and $K=0.0015$ and the experimental values for upper layer flows (Egashira·Ashida[6], 1979). The experimental ones, which are obtained from $\kappa_N=0.4$, are plotted in the figure. It will be found that the theory elucidates the data well.

Therefore, the change of Kármán constant would be calculated from equation (65) with $B=1$, $K=0.0015$ and $\kappa_N=0.4$ in stratified shear flows.

The foregoing theory could be applied to middle layer flows by using the velocity coefficient of middle layer type.

4. Density and Temperature Profiles of Density Stratified Flows

4.1 Density and Temperature Profiles

(1) Upper Layer Flows

Concerning water density and temperature, the profiles can be discussed by the same method as was the velocity one, using the mixing length theory. But the mixing lengths for mass and heat are not the same as that of momentum because of the difference of buoyancy effect between scalar and vector quantities. Generally, the mass or the heat mixing length will be influenced and decreased by density stratification more than will the momentum one.

Let's discuss the vertical distribution of density and temperature in an upper layer flow as shown in **Fig. 4**. In the figure, the distribution of mixing length for mass density is shown. Its distribution is supposed to be

$$l_\rho = l_{0\rho} + \kappa_\rho z \,. \tag{66}$$

Where $l_{0\rho}$: mixing length at interface for mass and κ_ρ: Kármán constant for mass but not the universal one. As for heat,

$$l_H = l_{0H} + \kappa_H z \tag{67}$$

where l_{0H} is the mixing length at the interface for heat and κ_H: Kármán constant for heat. With the turbulent flux for mass $(-\overline{\rho' w'})$ and heat $(-\overline{T' w'})$, the density and temperature gradients are shown respectively as follows.

$$\frac{d\rho}{dz} = \frac{-\overline{\rho' w'}}{(l_{0\rho} + \kappa_\rho z) u_*} \tag{68}$$

$$\frac{dT}{dz} = \frac{-\overline{T' w'}}{(l_{0H} + \kappa_H z) u_*} \tag{69}$$

Where ρ: the mass density and T: water temperature, which are averaged in time, respectively. In the condition of constant flux layer, the turbulent flux term can be written by equations (8b), (9) and (11), as follows.

$$-\overline{\rho' w'} = -1/2 \cdot K \Delta\rho U_1 / R_{i*} \tag{70}$$

$$-\overline{T' w'} = 1/2 \cdot K \Delta T U_1 / R_{i*} \tag{71}$$

Where $\Delta\rho = \rho_2 - \rho_1$ and $\Delta T = T_1 - T_2$. Substituting equations (70) and (71) for turbulent flux terms of equations (68) and (69), and integrating them under constant flux layer, we can get the laws of density and temperature profiles in the main flow region of the upper layer flow:

$$\rho(\zeta) = \rho_i - \frac{\Delta\rho}{2} \frac{K}{R_{i*}} \frac{U_1}{u_*} \frac{1}{\kappa_\rho} \ln \frac{\beta_\rho + \kappa_\rho \zeta}{\beta_\rho} \tag{72}$$

$$T(\zeta)=T_i+\frac{\Delta T}{2}\frac{K}{R_{i*}}\frac{U_1}{u_*}\frac{1}{\kappa_H}\ln\frac{\beta_H+\kappa_H\zeta}{\beta_H} \tag{73}$$

Where ζ is the same as the preceding chapter. β_ρ and β_H are the nondimensional mixing lengths at the interface for mass and heat, which are defined by

$$\beta_\rho=l_{0\rho}/d_1 \tag{74}$$

and

$$\beta_H=l_{0H}/d_1 \tag{75}$$

respectively. ρ_i and T_i are the density and temperature at an interface and nearly equal to

$$\rho_i=(\rho_1+\rho_2)/2 \tag{76}$$

and

$$T_i=(T_1+T_2)/2 \tag{77}$$

, respectively (Ashida·Egashira[4]).

(2) Middle Layer Flows

We will be able to obtain the profiles in the case of middle layer flow, supposing the distribution of the mixing lengths for mass and heat as shown in Fig. 5 and the constant flux layer. Here we would like to show the results only.

In the region from the second interface to maximum velocity point, we get

$$\rho(\zeta)=\rho_{iL}-\frac{\Delta\rho_L}{2}\frac{K}{R_{i*L}}\frac{U_2}{u_{*L}}\frac{1}{\kappa_{\rho L}}\ln\frac{\beta_{\rho L}+\kappa_{\rho L}\zeta}{\beta_{\rho L}},\quad(0\leq\zeta\leq1) \tag{78}$$

and

$$T(\zeta)=T_{iL}+\frac{\Delta T_L}{2}\frac{K}{R_{i*L}}\frac{U_2}{u_{*L}}\frac{1}{\kappa_{HL}}\ln\frac{\beta_{HL}+\kappa_{HL}\zeta}{\beta_{HL}},\quad(0\leq\zeta\leq1) \tag{79}$$

, where ζ is defined by z/d_L, $\Delta\rho_L$ and ΔT_L are the density and temperature differences between middle and lower layers, respectively, R_{iL}: the overall Richardson number defined by $\Delta\rho_L$, d_2 and U_2, u_{*L}: the shear velocity at the second interface, $\kappa_{\rho L}$ and κ_{HL}: Kármán constants for mass and heat. $\beta_{\rho L}$ and β_{HL} are the nondimensional mixing lengths at the second interface for mass and heat respectively, and these are defined as follows.

$$\beta_{\rho L}=l_{0\rho L}/d_L \tag{80}$$

$$\beta_{HL}=l_{0HL}/d_L \tag{81}$$

Where d_L is the layer depth from the second interface to the maximum velocity point, $l_{0L\rho}$ and l_{0HL}: mixing lengths at the second interface for mass and heat respectively.

In the region from the maximum velocity point to the first interface,

$$\rho(\eta)=\rho_{L1}-\frac{\Delta\rho_U}{2}\frac{K}{R_{i*U}}\frac{U_2}{u_{*U}}\frac{1}{\kappa_{\rho U}}\ln\frac{\beta_{\rho U}+\kappa_{\rho U}}{\beta_{\rho U}+\kappa_{\rho U}\eta} \tag{82}$$

and

$$T(\eta) = T_{L1} + \frac{\Delta T_U}{2} \frac{K}{R_{i*U}} \frac{U_2}{u_{*U}} \frac{1}{\kappa_{HU}} \ln \frac{\beta_{HU} + \kappa_{HU}}{\beta_{HU} + \kappa_{HU}\eta} \tag{83}$$

, where ρ_{L1} and T_{L1} are the quantities at the maximum velocity point and obtained from equations (78) and (79) with $\zeta = 1$, η: y/d_U, $\Delta\rho_U$ and ΔT_U: the density and temperature differences in cross mean between middle and upper layers, respectively, R_{i*U}: the overall Richardson number defined by $\Delta\rho_U$, d_2 and U_2, and u_{*U}: the shear velocity at the first interface. $\beta_{\rho U}$ and β_{HU} are the nondimensional mixing lengths at the first interface for mass and heat respectively, and are defined as follows.

$$\beta_{\rho U} = l_{0\rho U}/d_U \tag{84}$$

$$\beta_{HU} = l_{0HU}/d_U \tag{85}$$

Where $l_{0\rho U}$ and l_{0HU} are mixing lengths at the first interface for mass and heat, and d_U is the layer depth from the maximum velocity point to the first interface.

The profile laws have been described in the main flow region of the upper and the middle layer flows. If the nondimensional mixing lengths and Kármán constants are known, theories for the profiles will become complete. We would like to discuss these unknown quantities in other sections.

4.2 The Nondimensional Mixing Lengths at Interface for Mass and Heat

As mentioned in the preceding chapter, a strong stability region will be formed near the density interface. Therefore, the same manner as the one employed in section **3.2** could be used. Webb[3] also showed that the air temperature was described as

$$d\theta/dz = \alpha T_*/\kappa_N L \tag{86}$$

in the limit of log-linear law. Where θ is the potential temperature, κ_N: Kármán's universal constant (0.4), L: Monin·Obukhov length and T_*: the quantity which has the dimension of temperature:

$$T_* = H/\rho_a C_p u_* \tag{87}$$

, where H is the heat flux, ρ_a: mass density of air and C_p: specific heat at constant pressure. The above expression means that the temperature or density field is controlled by momentum and heat or mass flux only, and temperature or density profile becomes linear. The fact can be inferred from turbulent energy equations and has been shown by experiments.

According to Turner[18], the feature mentioned above can be written by

$$\frac{d\rho}{dz} = -\frac{\rho}{g} k_2^2 \frac{\overline{(g\rho' w'/\rho)^2}}{u_*^4} \tag{88}$$

, where k_2 is the proportional constant to be decided. If one uses equation (70) as to mass flux, the following expression can be obtained.

$$\frac{d\rho}{dz}=\frac{\rho}{g}\left(\frac{k_2K}{2}\right)^2\left(\frac{U_1}{u_*}\right)^4\left(\frac{U_1}{d_1}\right)^2. \tag{89}$$

Also, the density gradient can be shown by using equation (68) and (70) as follows.

$$\frac{d\rho}{dz}=-\frac{\Delta\rho}{2}\frac{K}{R_{i*}}\left(\frac{U_1}{u_*}\right)\frac{1}{l_{0\rho}} \tag{90}$$

From equations (89) and (90), the mixing length and its nondimensional one at the interface for mass can be obtained as

$$l_{0\rho}=\gamma_2(U_1/u_*)^{-3}d_1 \tag{91}$$

and

$$\beta_\rho=\gamma_2(U_1/u_*)^{-3} \tag{92}$$

respectively. Where γ_2 is the empirical constant and shown as

$$\gamma_2=2/(k_2^2K). \tag{93}$$

It is clear from equation (92) that the function of β_ρ is the same as the one for the momentum mixing length.

We can discuss the one for heat in the same manner. In the range where the heat expansion ratio is considered to be constant, the mixing length and the nondimensional one at an interface for heat is the same as the one for mass. The results are

$$l_{0H}=l_{0\rho} \tag{94}$$

and

$$\beta_H=\beta_\rho \tag{95}$$

respectively.

Fig. 8 shows the relation between equation (92) and the data obtained from

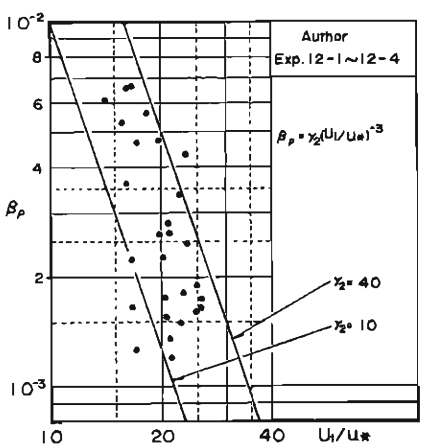

Fig. 8. The relation between the velocity coefficient and the nondimensional mixing length at a density interface for mass transfer.

the channel experiments[6] for the upper layer flow. As clear from the figure, the data being proportional to the inverse of the third power of velocity coefficient, the foregoing theory will be considered appropriate. The coefficient γ_2 of equation (92) lies in the range,

$$10 \leq \gamma_2 \leq 40 . \tag{96}$$

When one compares the results shown in **Fig. 6** and **Fig. 8**, it is found that β_ρ is smaller than β, and about a tenth of the momentum mixing length. It is considered that the buoyancy effect exerts influence on the mass and heat transfer more than on the momentum one.

Mixing lengths at the density interface for mass and heat having been discussed as to an upper layer flow, we can also obtain the ones for the middle layer flow. The results only are shown as follows.

$$\beta_{\rho U} = \beta_{HU} = \gamma_2 (U_2/u_{*U})^{-3} \tag{97}$$

$$\beta_{\rho L} = \beta_{HL} = \gamma_2 (U_2/u_{*L})^{-3} \tag{98}$$

4.3 Kármán Constants for Mass and Heat Mixing Lengths

The laws of mass density and temperature profiles have been obtained as equations (72) and (73), respectively. By integrating these formulae from the interface to water surface with respect to z, Kármán constants for mass and heat will be given automatically. That is, the structure of profiles are regulated by the cross sectional mean quantities.

Rearranging the relations obtained by the above method, we can get the following equations with respect to κ_ρ and κ_H in the upper layer flow.

$$\kappa_\rho = KF_i^2 \frac{U_1}{u_*} \frac{\beta_\rho + \kappa_\rho}{\kappa_\rho} \ln\left(\frac{\beta_\rho + \kappa_\rho}{\beta_\rho} - 1\right) \tag{99}$$

$$\kappa_H = KF_i^2 \frac{U_1}{u_*} \frac{\beta_H + \kappa_H}{\kappa_H} \ln\left(\frac{\beta_H + \kappa_H}{\beta_H} - 1\right) \tag{100}$$

In the preceding section, it is realized that β_ρ is equal to β_H. Therefore, the following relation will be sure if one compares equation (99) with (100).

$$\kappa_\rho = \kappa_H$$

This has led to the fact that the mixing length for mass is the same as the one for the heat, in other words, eddy diffusion coefficients for mass, heat and some solute are equal to one another. Such a fact has been recognized by channel experiments and field observations.

Let us investigate the relation between equation (99) and experiments. We can obtain the theoretical curve for Kármán constant of mass mixing length, applying equations (46) and (92) to U_1/u_* and β_ρ respectively. In **Fig. 9**, the families of curves, which can be calculated with $\kappa_{\rho N}=0.4$, $K=0.0015$, $A=15$, $(H-d_1)/H$ 0.5 and $\gamma_2=10$, are shown, and experimental values by Egashira·Ashida[6] are also plotted. $\kappa_\rho/\kappa_{\rho N}$ increases with internal Froude number in theory and experiments, because the stability effects decrease as F_i becomes large. Influences of Reynolds number on $\kappa_\rho/\kappa_{\rho N}$ appear remarkable in the range less than $R_*=10^4$, and becomes

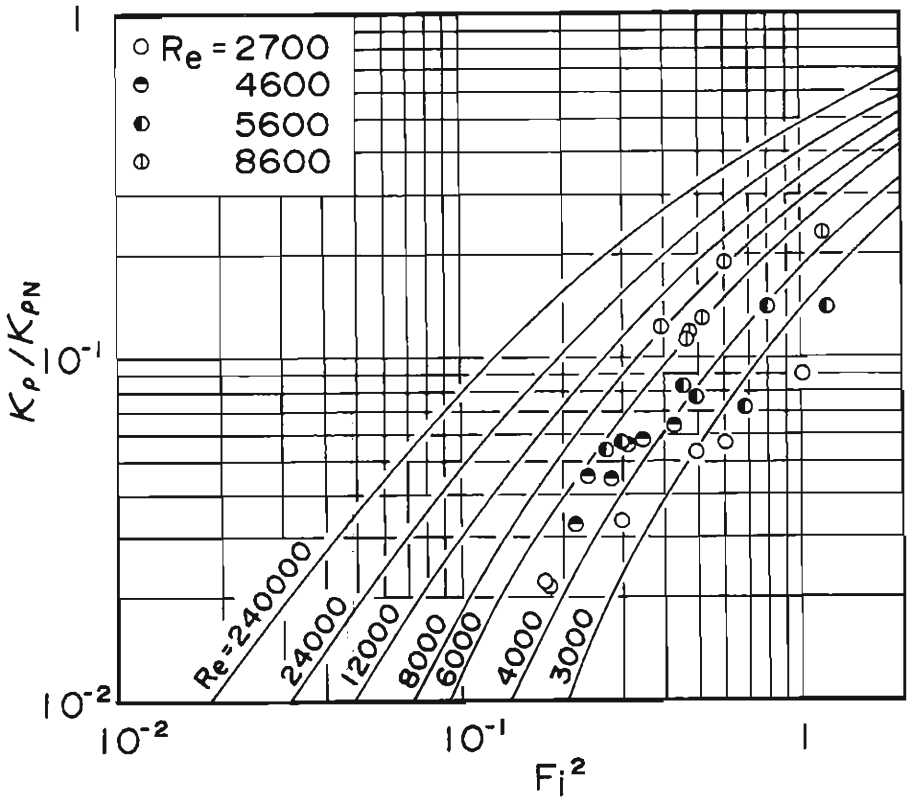

Fig. 9. The relation between internal Froude number and the ratio of Kármán constants concerning the mixing length for mass with Reynolds number as a parameter, where $\kappa_{\rho N}=0.4$.

negligible as its value goes beyond 10^5. The experimental values in the range of Reynolds number larger than 10^4 not being obtained, we cannot compare the theory and experiment in its wide range. It will be found that the families of curves agree well with experiments as far as the experimental values exist. Then, Kármán constant for mass and heat mixing lengths will be predicted by equation (99) or (100). We can easily obtain Kármán constants defined as $\kappa_{\rho U}$ and $\kappa_{\rho L}$ in the same manner, concerning a middle layer flow.

5. Eddy Diffusion Coefficient for Mass and Heat in Density Stratified Flow

Let us discuss the distribution of the vertical component only. We select the coordinate system as shown in **Fig. 4**, and then can write the eddy diffusion coefficient of gradient type for mass and heat by the use of mixing length and shear velocity, as follows.

$$\varepsilon_{\rho z}=l_\rho u_*=(l_{0\rho}+\kappa_\rho z)u_* \tag{101}$$

where l_ρ is the mixing length for mass and equal to that for heat. Consequently,

$$\varepsilon_{\rho z}=\varepsilon_{Hz} \tag{102}$$

where ε_{Hz} is the one for heat. Then, that for mass will be only related below. Now then, substituting equation (91) for $l_{0\rho}u_*$ in equation (101), and using the continuity as shown by $q=U_1d_1$, one can obtain the following relation.

$$\varepsilon_{\rho\zeta}=\left\{\gamma_2\left(\frac{U_1}{u_*}\right)^{-3}+\kappa_\rho\zeta\right\}\left(\frac{U_1}{u_*}\right)^{-1}q \tag{103}$$

where ζ is defined by z/d_1 as previously mentioned.

The first term is the eddy diffusion coefficient at interface, and it is shown as

$$\varepsilon_{\rho i}=\gamma_2(U_1/u_*)^{-4}q \tag{104}$$

The above formula can also be obtained from equations (14), (90) and (91). By substituting equation (46) for U_1/u_*, equation (104) is transformed into

$$\frac{\varepsilon_{\rho i}}{q}=\frac{\gamma_2}{4}\left\{\frac{A}{R_e}+0.00207F_i^2+K\frac{H-d_1}{H}\right\}^2 \tag{105}$$

In **Fig. 10**, the families of curves which can be obtained from equation (105) with $\gamma_2=10$, $K=0.0015$, $(H-d_1)/H=0.5$ and $A=1.86$ and $A=15$, are shown. It will be clear from the figure that the eddy diffusion coefficient normalized by unit width discharge is influenced by Froude number only as far as Reynolds number is large and the depth ratio keeps constant. On the other hand, the coefficient approaches the molecular one as the Reynolds number becomes small. We cannot discuss the characteristics of equation (105) in the molecular range because the theory is in the turbulent region as made clear in the description of the preceding chapters.

Let us focus on equation (103) again. As clear in **Fig. 9** and **Fig. 10**, Kármán constant and the inverse of velocity coefficient increase with Froude number. Consequently, the eddy diffusion coefficient indicated by equation (103) increases in the main flow region in accordance with increase of Froude number. The coefficient becomes large linearly as the position under consideration goes further away from the interface, and is maximum at the free surface. But the theory could not be applied in the region near surface because it was established under constant flux layer, that is, the assumption of constant flux layer is not relevant there.

The eddy diffusion coefficient in a cross sectional mean can be obtained by integrating equation (103) as follows.

$$\varepsilon_{\rho m}=\left\{\gamma_2\left(\frac{U_1}{u_*}\right)^{-3}+\frac{1}{2}\kappa_\rho\right\}\left(\frac{U_1}{u_*}\right)^{-1}q \tag{106}$$

where $\varepsilon_{\rho m}$ is the cross sectional mean of the eddy diffusion coefficient.

Eddy diffusion coefficient for mass and heat has been discussed on the basis of the distribution of the mixing length realized in the preceding chapter. In the same manner, that for the momentum can be obtained as follows.

$$\varepsilon_\zeta=\left\{\gamma_1\left(\frac{U_1}{u_*}\right)^{-3}+\kappa\zeta\right\}\left(\frac{U_1}{u_*}\right)^{-1}q \tag{107}$$

where ε_ζ is the eddy diffusion coefficient for momentum. If one compares the result

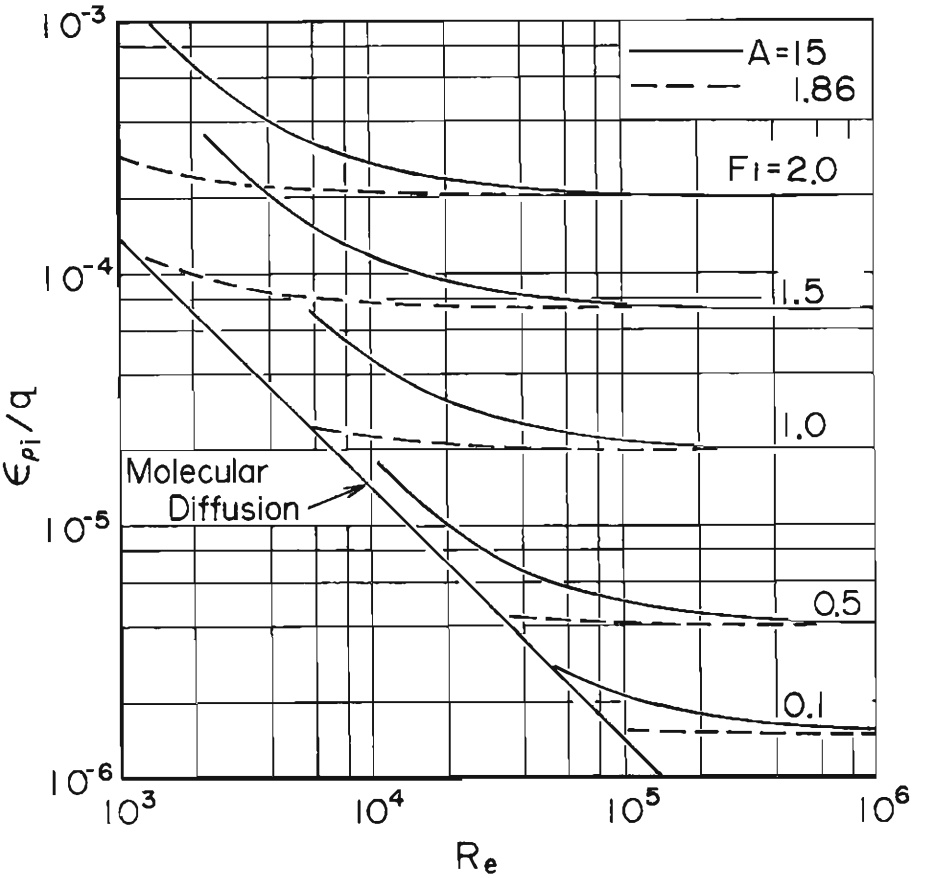

Fig. 10. Eddy diffusion coefficient at a density interface for mass and heat. The coefficient is normalized by the discharge in unit width. Molecular diffusion coefficient shown on the figure is the value at 20°C in water temperature.

shown in Fig. 7 with the one in **Fig. 9**, and γ_1 with γ_2, that is, if one compares equation (107) with (103), it will be found that ε_ζ is greater than $\varepsilon_{\rho\zeta}$. Consequently, turbulent Prandtl number which is defined as $P_r=\varepsilon_\zeta/\varepsilon_{\rho\zeta}$ will be much larger than the factor of one in the density stratified flow. Therefore, the heat transfer in the vertical direction can be suppressed extremely. Then, the formation of the layer, a kind of heat boundary layer, which we call "Thermal Boundary Layer" here, is restrained as a result, and on the other hand the shear layer for momentum extends to the free surface at a short distance from the upstream end. If we want to know the diffusion coefficient for heat or some solute where the thermal boundary layer is not formed yet, we had better use the following formula obtained from substituting κ for κ_ρ.

$$\varepsilon_{\rho\zeta}=\left\{\gamma_2\left(\frac{U_1}{u_*}\right)^{-3}+\kappa\zeta\right\}\left(\frac{U_1}{u_*}\right)^{-1}q \tag{108}$$

Concerning the middle layer flow, we can easily discuss the eddy diffusion coefficient by the same manner as before. The result only is shown below.

$$\varepsilon_{\rho\eta}=\left\{\gamma_2\left(\frac{U_2}{u_{*U}}\right)^{-3}+\kappa_{\rho U}\eta\right\}\left(\frac{U_2}{u_*}\right)^{-1}q\frac{d_U}{d_2} \tag{109}$$

$$\varepsilon_{\rho\zeta}=\left\{\gamma_2\left(\frac{U_2}{u_{*L}}\right)^{-3}+\kappa_{\rho L}\zeta\right\}\left(\frac{U_2}{u_{*L}}\right)^{-1}q\frac{d_L}{d_2} \tag{110}$$

where the coordinate systems are the same as the preceding chapter. On the other hand, in the region where the thermal boundary layer is not formed, the above relations become

$$\varepsilon_{\rho\eta}=\left\{\gamma_2\left(\frac{U_2}{u_{*U}}\right)^{-3}+\kappa_U\eta\right\}\left(\frac{U_2}{u_{*U}}\right)^{-1}q\frac{d_U}{d_2} \tag{111}$$

and

$$\varepsilon_{\rho\zeta}=\left\{\gamma_2\left(\frac{U_2}{u_{*L}}\right)^{-3}+\kappa_L\zeta\right\}\left(\frac{U_2}{u_{*L}}\right)^{-1}q\frac{d_L}{d_2} \tag{112}$$

respectively.

6. Relation between Theory and Experiment

6.1 Velocity and Temperature Profiles

(1) Upper Layer Flows

The experimental flume which is 23 meters in length, 38.5 centimeters in width and 70 centimeters in depth is used. The channel floor is sloped 1.0 percent. Experiments were carried out by the following method. Filling the channel with water to the level of the weir which is attached to the downstream end, we have the heated water flow into the flume from the upstream end at constant discharge and have it overflow at the downstream end. An upper layer flow can be formed by such a method. As soon as overflow begins from the weir at the downstream end, inflow and overflow water temperature, and the profiles of velocity and temperature at two cross sections are measured. The profile of water temperature was measured by thermista probes at two sections which were situated 5.5 and 12.8 meters from the downstream end. Velocity profiles were measured by the hydrogen bubble method at two sections 4.3 and 11.5 meters from the downstream end, respectively.

Experimental results and the theoretical curves are shown in **Fig. 11(a)**, **(b)**, **(c)** and **(d)** of which discharges in unit width are 22.86, 39.74, 49.09 and 76.62 cm²/sec in that order. **U** in the figure means the results at the sections 12.8 meters for temperature and 4.3 meters for velocity, and **D** means the ones 5.5 meters for temperature and 4.3 meters for velocity, respectively. The theoretical curves are obtained from equations (18) and (24) for velocity profile and (79) for temperature, together with equations (19), (54), (65), (73) and (100) which are employed to calculate u_*, β, κ, β_E and κ_E.

It is clear from the figure that the theories accord fairly well with the experiments in spite of the ones under the assumption of constant flux layer. But the following problems may exist: As to velocity profiles, the theory gives the shape flatter than that of the experiment as shown in **Fig. 11(a)** of which discharge is the least of the four cases and its Reynolds number is about 2700. We think that the

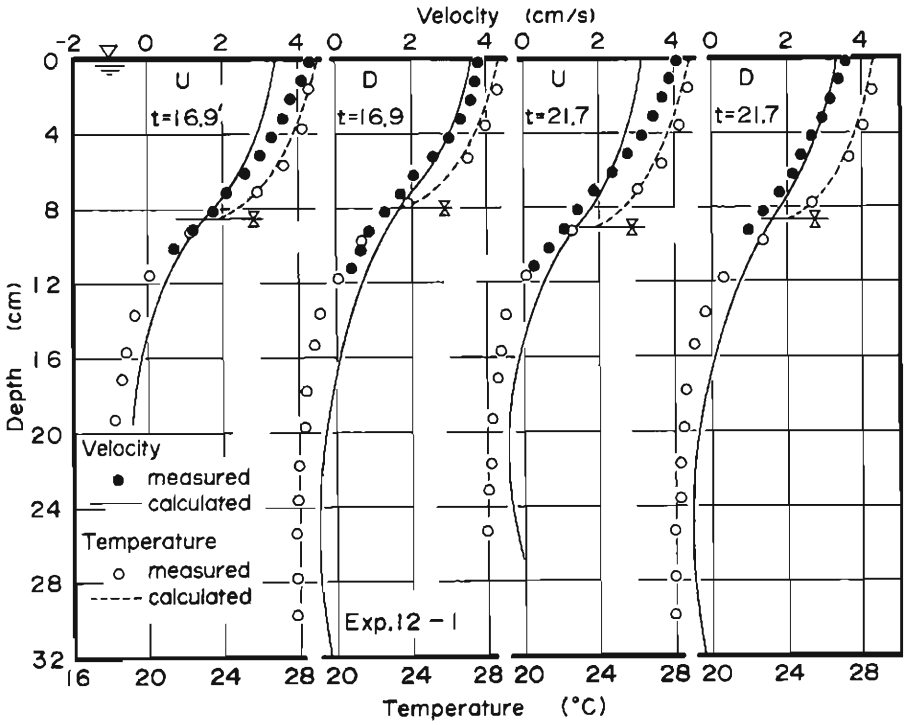
Velocity (cm/s)
U
t=16.9'
D
t=16.9
U
t=21.7
D
t=21.7
Depth (cm)
Velocity
measured
calculated
Temperature
measured
calculated
Exp.12 – 1
Temperature (°C)

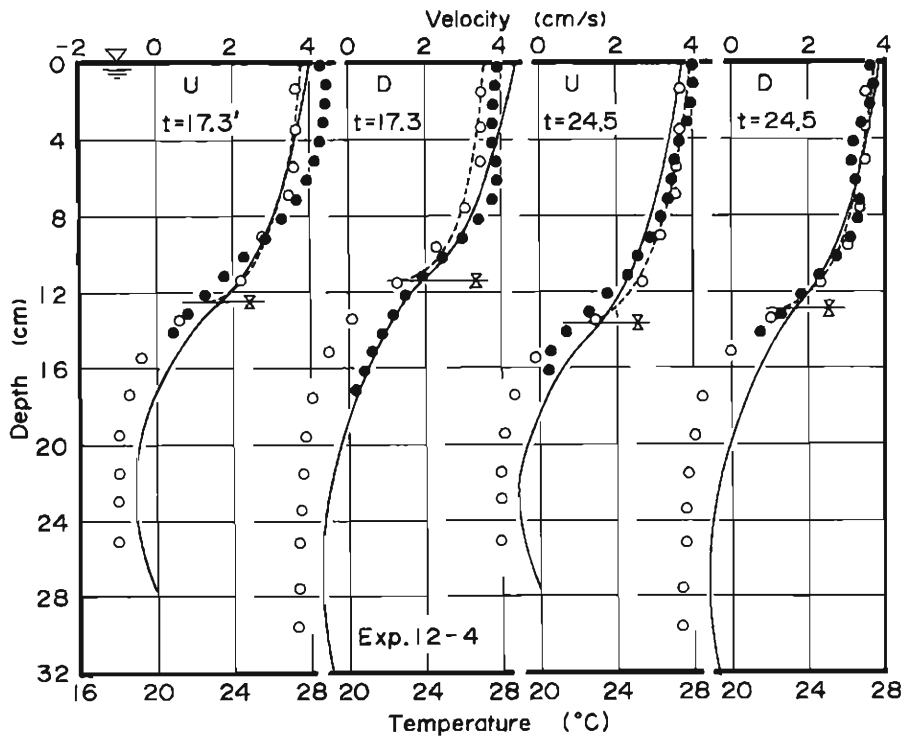
Velocity (cm/s)
U
t=17.3'
D
t=17.3
U
t=24.5
D
t=24.5
Depth (cm)
Exp.12-4
Temperature (°C)

Fig. 11 (a), (b)

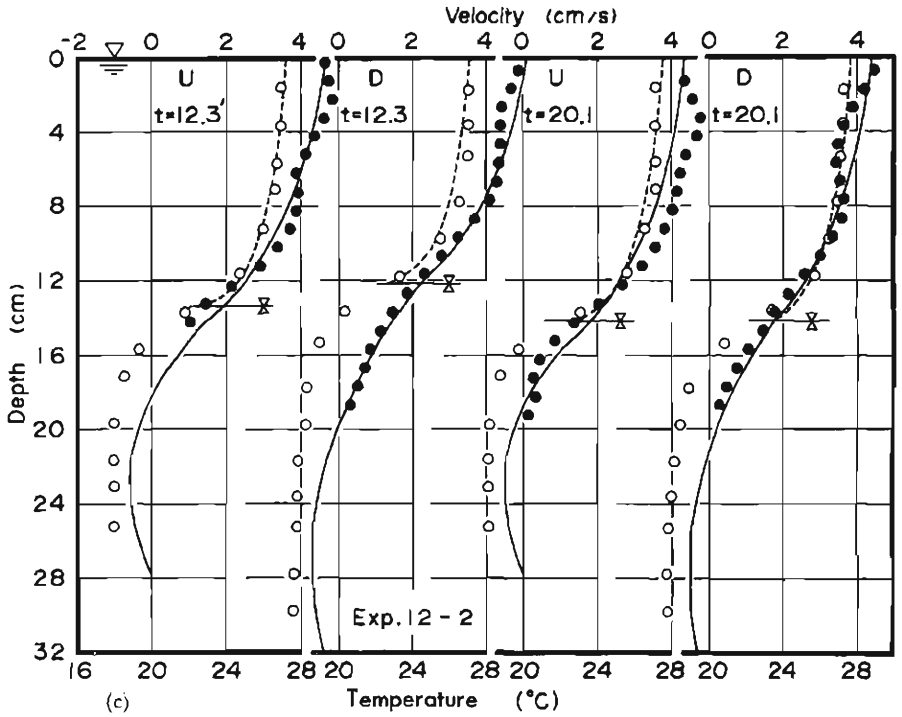

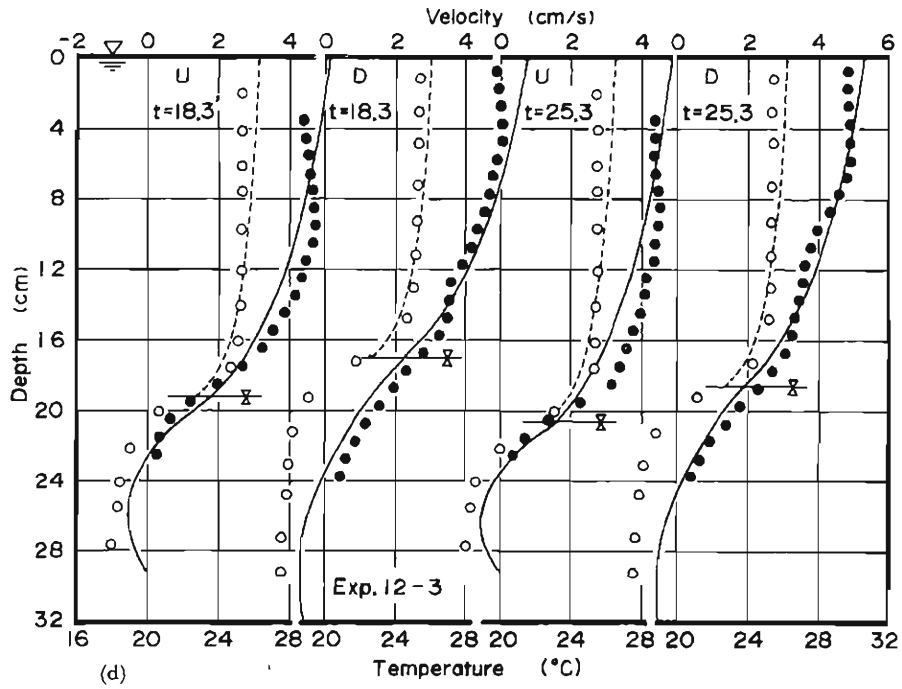

Fig. 11 (a), (b), (c), (d). Comparison between theory and experiment concerning the velocity and temperature profiles in upper layer flows.

discrepancy is caused for the following reasons: One is consider to be experimental error because the discharges calculated from the profiles at two sections are different from each other. The other is for the applicability of theory because it may be possible or not for us to treat the turbulent shear flow such a flow of small Reynolds number. Concerning the temperature profiles, it is an important problem whether a thermal boundary layer will be formed at the free surface or not. The larger are Prandtl and Reynolds numbers, the more the layer is suppressed. The thermal boundary layer is also suppressed for the sake of secondary flow caused by the small aspect ratio. Concentrating our attention on these problems, and looking at the results in **Fig. 11(d)**, we will find that the law of water temperature represents the result of experiment at the downstream section (Section-**D**) much better than at Section-**U**.

(2) Middle Layer Flows

A middle layer flow can be formed by the following method, using the same flume as mentioned above. At first, filling the channel with water to a given level, and heating the water electrically or by natural solar radiation, we quietly supply water of temperature lower than the heated one to any level from the lowest

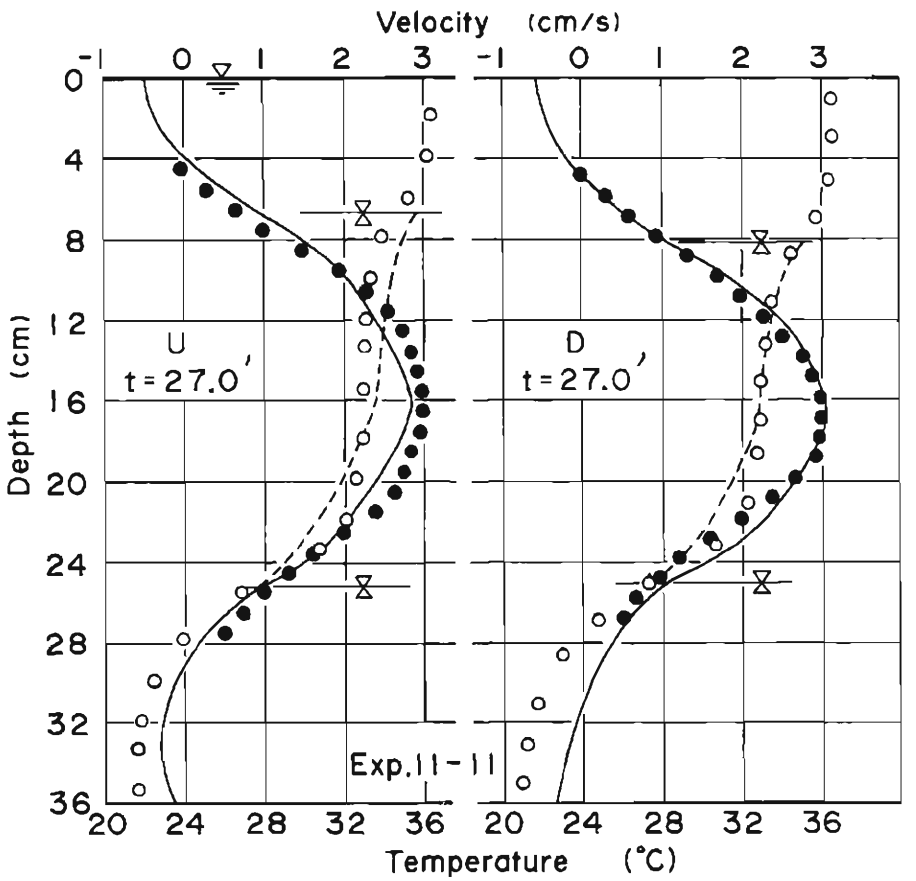

Fig. 12(a)

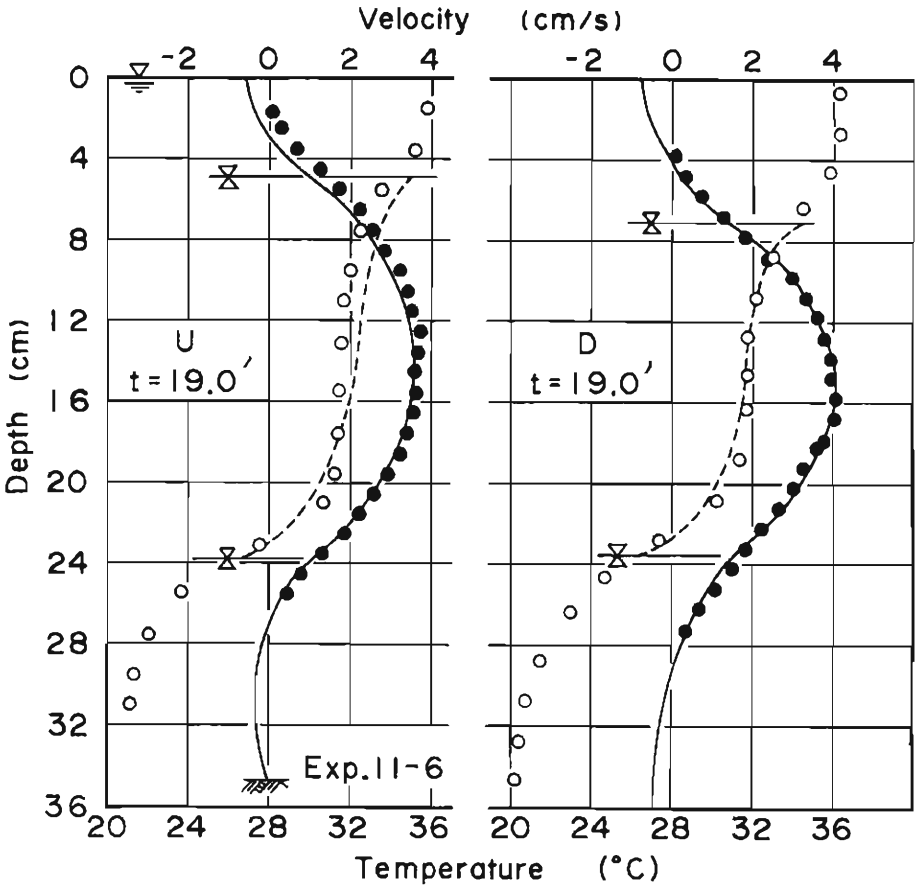

Fig. 12(b)

intake work attached to the downstream end. In this manner, some kind of temperature stratification can be formed in the experimental flume. Then, we have the water, which temperature is lower than that of the surface and higher than that of the lower region, inflow into the flume, and it outflow from the intake work at the middle depth of the downstream end, and then get a middle layer flow. After such a flow is obtained, hydraulic quantities of various kinds as mentioned in the preceding upper layer flow are measured.

The relation between theory and experiment concerning the velocity and temperature profiles is shown in **Fig. 12(a)**, **(b)** and **(c)** of which discharges are 40.0, 51.94 and 67.01 cm²/sec, respectively. Theoretical curves in the figures are obtained completely from the laws of profiles and supplementary equations as shown in the foregoing chapters, using the same coefficients as in the case of upper layer flow, that is, $\gamma_1=120$, $\gamma_2=10$, $A=15$, $K=0.0015$ and $B=1$.

When one compares the results in the figure, it will be found that the theories are well applied to the experiments concerning the velocity profiles in both section-**U** and section-**D**. It seems to say so as well for the temperature profiles, but actually it appears that the theories represent the experiments better in the section-**D** than in the

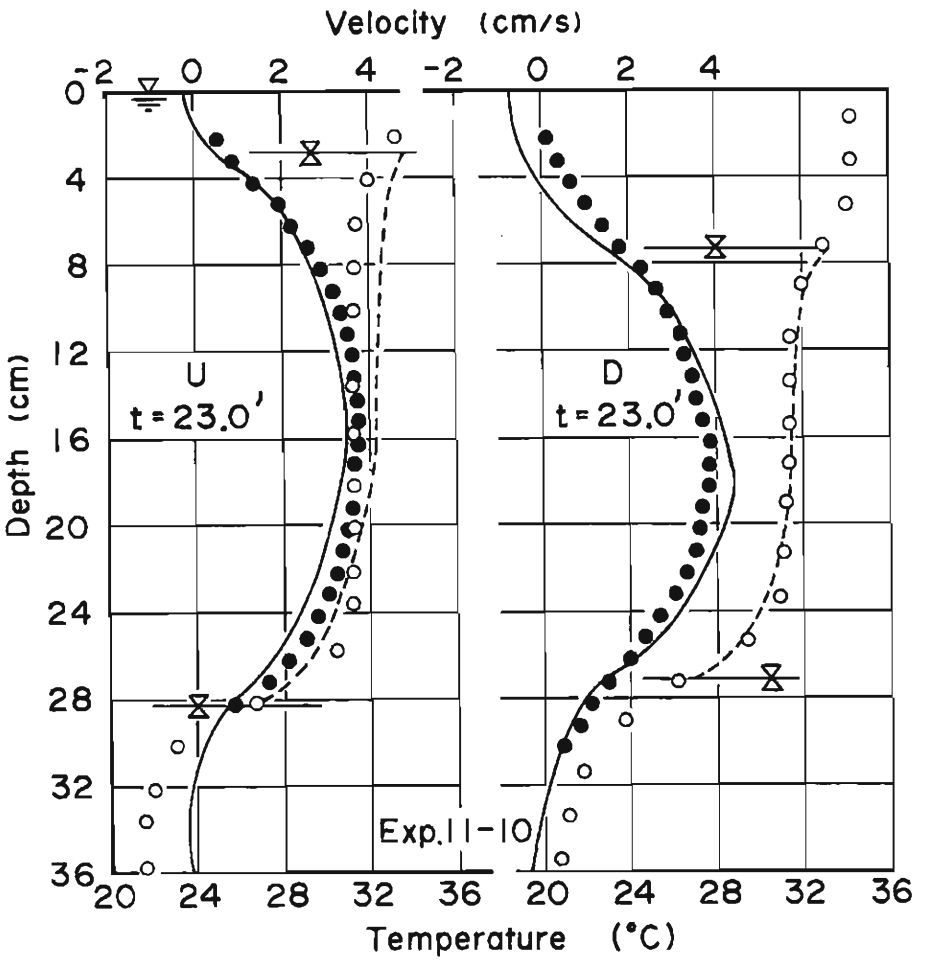

Fig. 12(c)

Fig. 12(a), (b), (c). Comparison between theory and experiment concerning the velocity and temperature profiles in middle layer flows.

section-**U**, because the thermal boundary layer is developed in the downstream more than in the upstream.

The relation between theory and experiment concerning the upper and middle layer flows has been discussed as described above. Although some problems on the limit of application of theory and on the thermal boundary layer may exist, the degree of the discrepancy between the theoretical and experimental values will be considered practically permissible.

6.2 Eddy Diffusion Coefficient

The experimental flume is the same as before and data is obtained from a tracer method as follows. A solution of potassium permanganate is injected into the stratified flows continuously at a given level in depth from a dynamic pressure Pitot tube, and the tracer is photographed at two second intervals by the interval

camera from the channel side. Simultaneously, velocity and temperature profiles are measured by the foregoing procedures.

Three cases of experiments for the upper layer flow and two cases for the middle layer flow were carried, respectively. An example of the diffusion of the tracer is shown in **Photo. 1**. If one evaluate the diffusion width of the envelope of

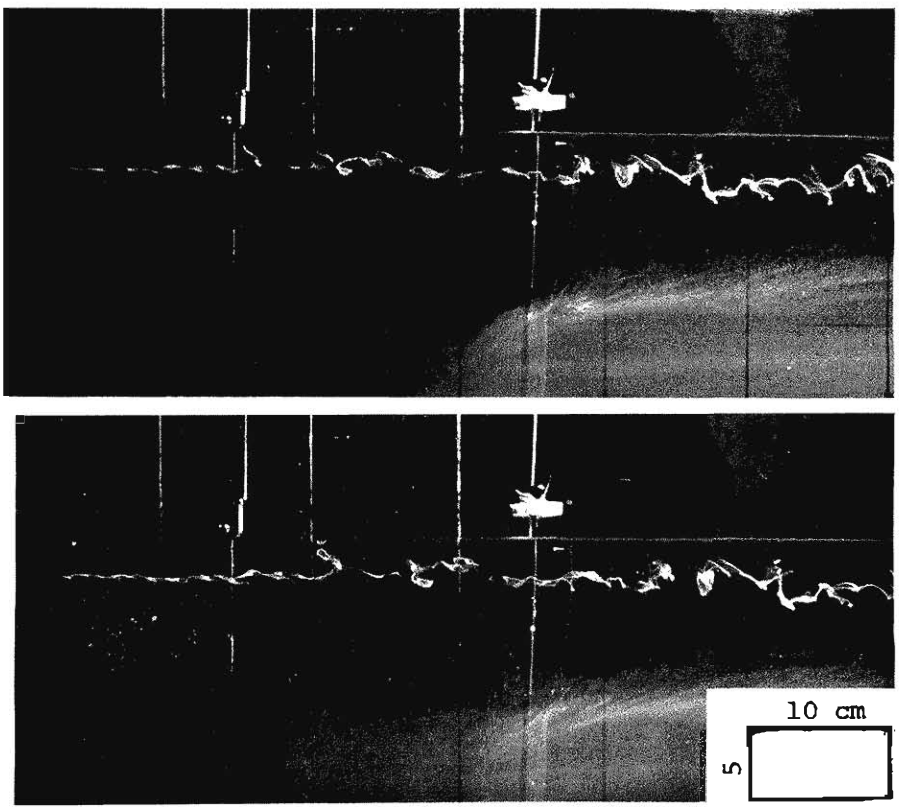

Photo. 1. An example of diffusion of tracer in an upper layer flow. The time interval between the two photographs is two seconds.

the tracer, $\sqrt{\overline{Y}}$, the eddy diffusion coefficient can be calculated by the following formula.

$$\varepsilon_{ztr}=\frac{1}{2}\frac{d}{dt}\overline{Y}^2 \tag{113}$$

where ε_{ztr}: z-component of diffusion coefficient of tracer. The above relation is used in order to calculate the diffusion coefficient in the flow of homogeneous and isotropic turbulence. On the other hand, the flow under consideration is that of a turbulent shear flow. Consequently, it should be noticed that equation (113) gives only an approximate value for the shear flow.

In **Fig. 13(a)**, **(b)** and **(c)**, the experimental values obtained from equation (113) and the theoretical ones predicted by the formulae in chapter **5** are shown, and pro-

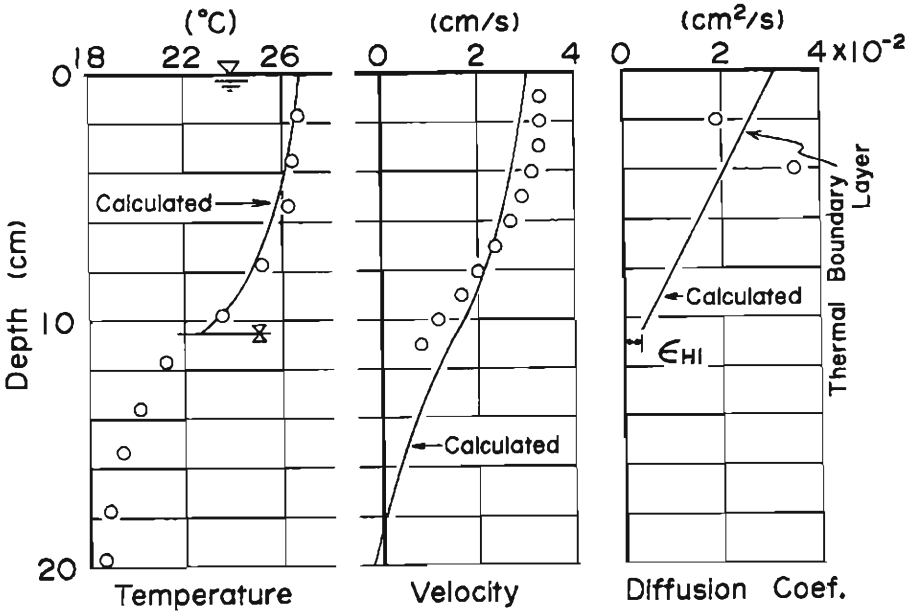

Fig. 13(a)

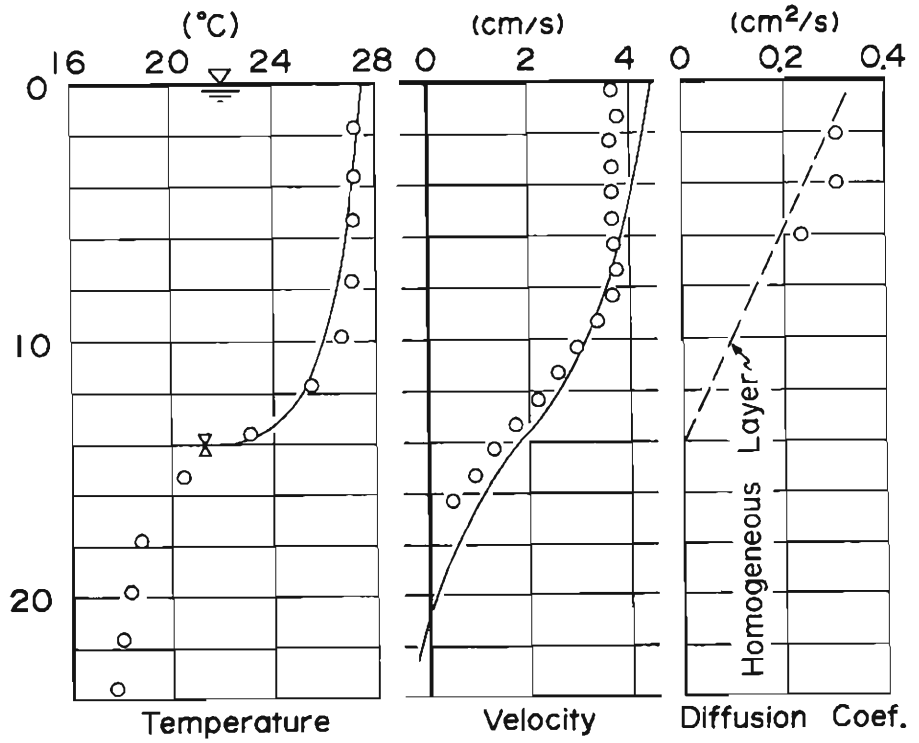

Fig. 13(b)

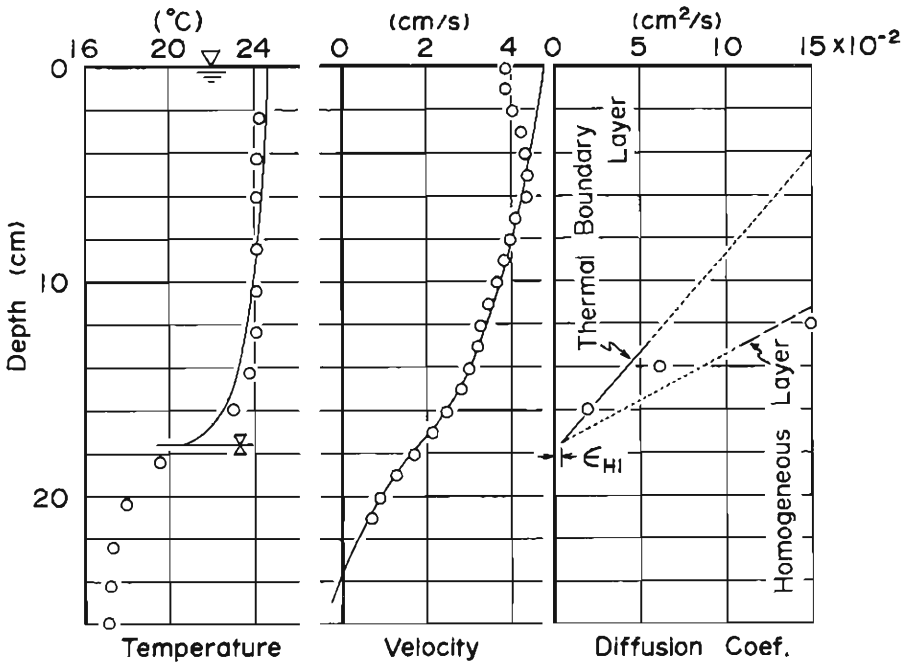

Fig. 13(c)

Fig. 13(a), (b), (c). Theoretical lines and experimental values of eddy diffusion coefficient for tracer concerning upper layer flows. Here, the eddy diffusion coefficient for tracer is thought to be equal to the one for mass and heat.

files of velocity and temperature are also shown. **Fig. 13(a)** is an example of the measured points inside the thermal boundary layer (TBL), and then the theoretical line is calculated from equation (103). The measured points which are situated outside TBL are shown in **Fig. 13(b)**, and in the figure the theoretical one is calculated by equation (108). **Fig. 13(c)** shows an example: One of the measuring points is outside TBL and the others inside it.

Referring to the results shown on the lefthand side of these figures concerning the temperature profiles predicted and measured, one will find that the measured values inside TBL can be predicted well by equation (103) and the ones outside it by equation (108), respectively.

In **Fig. 14**, an example concerning the middle layer flow is shown. One measured point is inside TBL and the other is outside it. The predicted lines are calculated by equations (109) and (111) respectively in the figure. The experimental value in the figure which is measured outside TBL, where the temperature gradient is nearly zero and consequently the buoyancy effect may be very little, can also well be represented by the equation (111), which is introduced by using κ_U instead of κ_ρ in equation (109).

We would like to investigate the relation between all data inside and outside TBL and theory. The relations between the data and theory as to upper layer flows are shown in **Fig. 15(a)** and **(b)**, and those of middle layer flows are compared

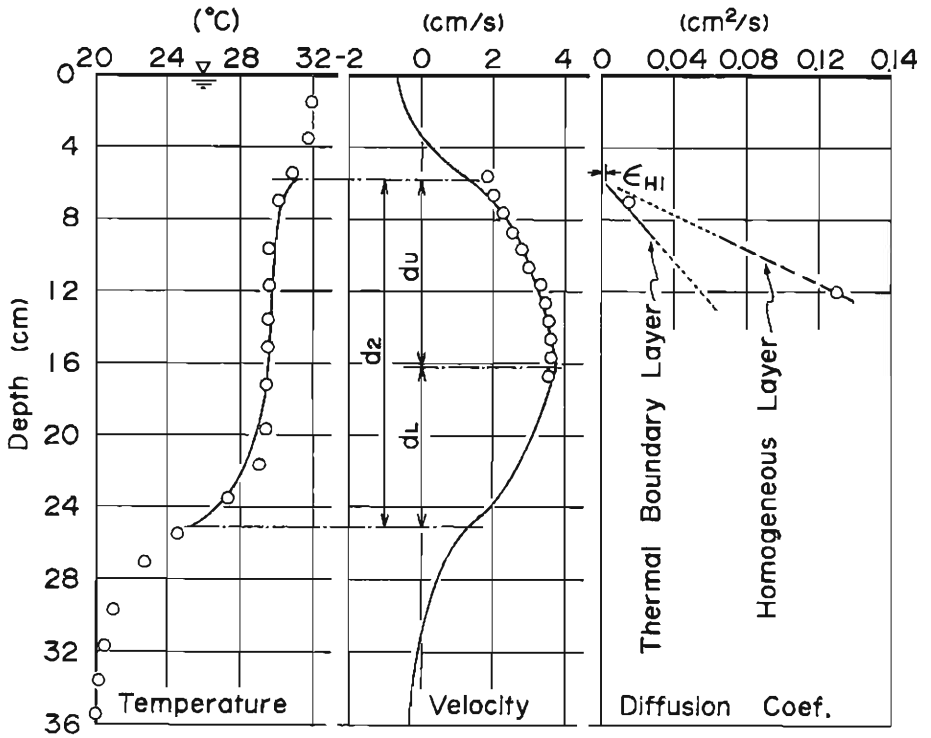

Fig. 14. Theoretical lines and experimental values of eddy diffusion coefficient for tracer in the middle layer flow. Here, the eddy diffusion coefficient for tracer is thought to be equal to the one for mass and heat.

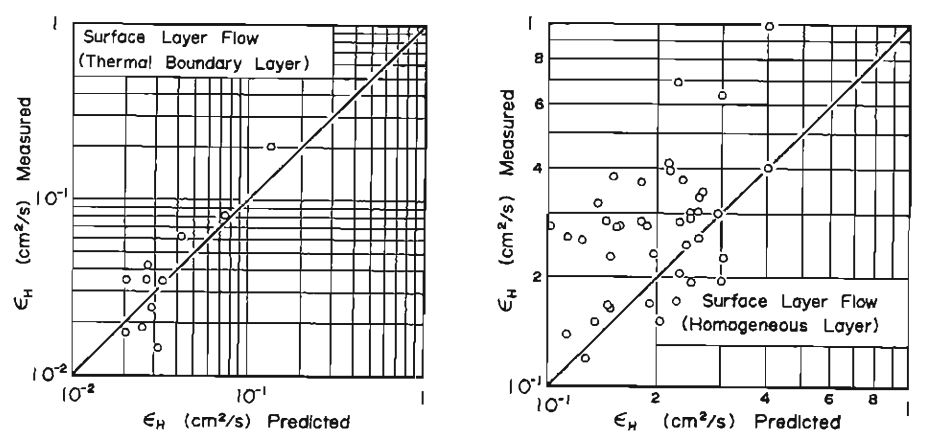

Fig. 15(a), (b). Comparison between theoretical and experimental values of eddy diffusion coefficient for mass and heat(=tracer) in upper layer flows.

in **Fig. 16(a)** and **(b)**, respectively. It will be clear from the figures that the theories developed in the regions of inside and outside TBL show good agreement with the experimental values for the diffusion coefficients.

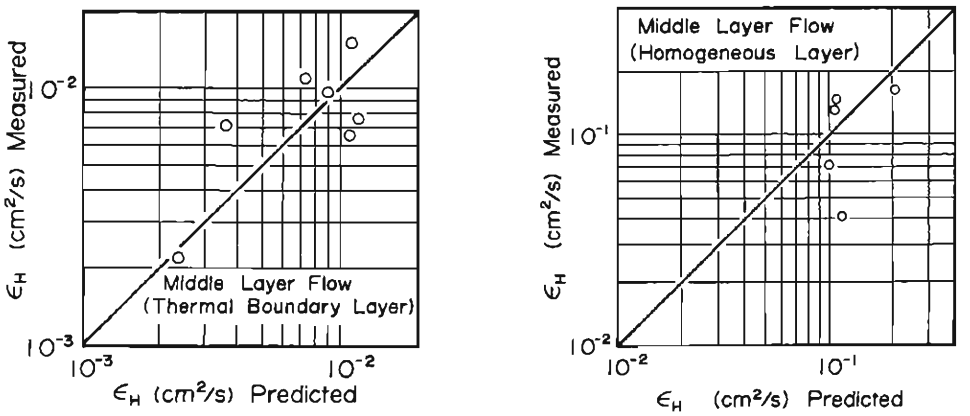

Fig. 16(a), (b). Comparison between theoretical and experimental values of eddy diffusion coefficient for mass and heat(=tracer) in middle layer flows.

7. Conclusion

We have discussed the velocity, density and temperature profiles and eddy diffusion coefficients in density stratified shear flows, and have obtained many interesting results from theoretical and experimental considerations, as follows.

(1) The relation between turbulent (eddy) diffusion coefficient at a density interface and turbulent entrainment one has been obtained, using the mass conservation equation expressed by convected diffusion terms in a continuous model and the one expressed by entrainment in a discrete model. The formula plays an important role in the discussions taken up in the latter chapters because the transfer conditions at an interface for mass and heat can be decided by the relation.

(2) We put the momentum mixing length l_0 to a density interface and assume the linear distribution of mixing length in main flow region, the profile laws of velocity and temperature have been obtained under conditions of constant flux layer. These profile laws are characterized by nondimensional mixing length at an interface and Kármán constant. The functional relationship of nondimensional mixing length is discussed with the result (1) and the condition of self-regulated state, and it is realized. In order to discuss Kármán constant, the new acceleration balance equation is introduced according to Kao, and its constant is clarified.

(3) The density and temperature profiles are also discussed on the basis of mixing length theory for mass and heat by assuming the distribution of mixing lengths as like the one for momentum. The functional relationship of nondimensional mixing length at interface is obtained in the same manner as the one for momentum. Concerning Kármán constants for mass and heat mixing lengths, the integral method is used in order to realize them.

(4) The distribution of eddy diffusion coefficients for mass and heat are discussed, using the distribution of mixing length clarified already and the shear velocity. The functional relationships are clarified in the main flow region covered by the thermal boundary layer. In the experiment carried out usually TBL is not developed enough because channel length is definite and turbulent Prandtl number is

large. In order to predict the diffusion coefficient in such a region, alternative formulae are proposed.

(5) Theories presented in this study have been evaluated by experiments.

Many interesting features of density stratified shear flows have been clarified. But the problems to be solved are left to future investigation. Especially, we must make efforts in order to clear up the applicability of these theories and the formation of a thermal boundary layer.

Acknowledgment

This study has been part of a research projected entitled "Study on Turbid water Problems in Reservoirs" (Representative: S. Adachi, Prof. of Nagoya Univ.) supported by the Natural Science Research Group under Ministry of Education. This support is gratefully acknowledged. We are also grateful to Mr. Y. Yoshida for his help in the experiments.

References

1) Lumley, J. L. and H. A. Panofsky: The Structure of Atmospheric Turbulence, John Wiley & Sons, 1964, pp. 99–118.
2) McVehill, G. E.: Wind and Temperature Profiles near the Ground in Stable Stratification, Qurt. Jour. Roy. Soc. Vol. 90, 1964, pp. 136–146.
3) Webb, E. K.: Profile Relationships: The Log-Linear Range, and Extension to Strong Stability, Qurt. Jour. Roy. Soc. Vol. 96, 1970, pp. 67–90.
4) Ashida, K. and S. Egashira: Studies on the Turbid Water Flows in Stratified Reservoirs(3) — Flow Pattern and Mixing Process —, D.P.R.I. of Kyoto Univ. Annuals. No 20B–2, 1977, pp. 437–450. (in Japanese)
5) Ashida, K. and S. Egashira: Velocity Profile of Stably Stratified Density Currents, D.P.R.I. of Kyoto Univ. Annuals. No 21B–2, 1978, pp. 455–465. (in Japanese)
6) Egashira, S. and K. Ashida: Structures of Density Stratified Flows, D.P.R.I. of Kyoto Univ. Annuals, No 22B–2, 1979, pp. 355–381. (in Japanese)
7) Hino, M.: Velocity Distribution and Interfacial Friction of Two-Layered Flow, Proc. of the 23rd Jap. Con. on Hydraulics, 1979, pp. 347–353. (in Japanese)
8) Munk, W. H. and E. R. Anderson: Note on a Theory of the Thermocline, Jour. Marine Res., Vol. 7, 1948, pp. 276–295.
9) Ellison, T. H.: Turbulent Transport of Heat and Momentum from an Infinite Rough Plane, Jour. Fluid Mech. Vol. 2, 1957, pp. 456–466.
10) Ellison, T. H. and J. S. Turner: Mixing of Dense Fluid in a Turbulent Pipe Flow, Part 2, Dependence of Transfer Coefficients on Local Stability, Jour. Fluid Mech., Vol. 8, 1960, pp. 529–544.
11) Launder, B. E.: On the Effects of a Gravitational Field on the Turbulent Transport of Heat and Momentum, Jour. Fluid Mech., Vol. 67, 1975, pp. 569–581.
12) Kato, H. and O. M. Phillips: On the Penetration of a Turbulent Layer into Stratified Fluid, Jour. Fluid Mech., Vol. 37, 1967, pp. 643–655.
13) Moore, M. T. and R. R. Long: An Experimental Investigation of Turbulent Stratified Shearing Flow, Jour. Fluid Mech., Vol. 49, 1971, pp. 635–655.
14) Ashida, K. and S. Egashira: Hydraulic Characteristics of Thermocline in Reservoirs, 17th Cong. of IAHR, Vol. 2, 1977, pp. 33–40.
15) Lofquist, K.: Flow and Stress Near an Interface between Stratified Liquids, The Physics of Fluids, Vol. 3, 1960, pp. 158–175.

16) Ellison, T. H. and J. S. Turner: Turbulent Entrainment in Stratified Flows, Jour. Fluids Mech., Vol. 6, 1959, pp. 423–448.
17) Ashida, K. and S. Egashira: Basic Study on Turbidity Currents, Proc. of JSCE, No. 237, 1975, pp. 37–50. (in Japanese) or Trans. of JSCE, Vol. 7, Hydraulic and Sanitary Engineering Div., pp. 83–86.
18) Turner, J. S.: Buoyancy Effects in Fluids, Cambridge Univ. Press, 1973, p. 137.
19) Komatsu, T.: Study of Flow Properties and Turbulence in a Stratified Shearing Flow, Docter Thesis Presented to Kyushu Univ., 1978, pp. 54–96. (in Japanese)
20) Kao, S. K.: Turbulent Transfer in the Boundary Layer of a Stratified Fluid, Jour. of Met., Vol. 16, 1959, pp. 497–503.
21) Hino, M.: On the Changes of Turbulent Structure in Suspended Solids Laden Flow, Proc. of JSCE, No. 92, 1963, pp. 11–20. (in Japanese)